10 Active Galactic Nuclei

W. N. Brandt, Scott F. Anderson, D. R. Ballantyne, Aaron J. Barth, Robert J. Brunner, George Chartas, Willem H. de Vries, Michael Eracleous, Xiaohui Fan, Robert R. Gibson, Richard F. Green, Mark Lacy, Paulina Lira, Jeffrey A. Newman, Gordon T. Richards, Donald P. Schneider, Ohad Shemmer, Howard A. Smith, Michael A. Strauss, Daniel Vanden Berk

Although the numbers of known quasars and active galactic nuclei (AGN) have grown considerably in the past decade, a vast amount of discovery space remains to be explored with much larger and deeper samples. LSST will revolutionize our understanding of the growth of supermassive black holes with cosmic time, AGN fueling mechanisms, the detailed physics of accretion disks, the contribution of AGN feedback to galaxy evolution, the cosmic dark ages, and gravitational lensing. The evolution of galaxies is intimately tied with the growth and energy output from the supermassive black holes which lie in the centers of galaxies. The observed correlation between black hole masses and the velocity dispersion and stellar mass of galaxy bulges seen at low redshift (Tremaine et al. 2002), and the theoretical modeling that suggests that feedback from AGN regulates star formation, tell us that AGN play a key role in galaxy evolution.

The goal of AGN statistical studies is to define the changing demographics and accretion history of supermassive black holes (SMBHs) with cosmic time, and to relate these to the formation and evolution of galaxies. These results are tightly coupled to the evolution of radiation backgrounds, particularly the ultraviolet ionizing background and extra-Galactic X-ray background, and the co-evolution of SMBHs and their host galaxies. The LSST AGN sample (§ 10.1) will be used by itself and in conjunction with surveys from other energy bands to produce a measurement of the AGN luminosity function and its evolution with cosmic time (§ 10.2) and the evolution of the bolometric accretion luminosity density. LSST will break the luminosity-redshift degeneracy inherent to most flux-limited samples and will do so over a wide area, allowing detailed explorations of the physical processes probed by the luminosity function. Indeed, the AGN sample will span a luminosity range of more than a factor of one thousand at a given redshift, and will allow detection of AGN out to redshifts of approximately seven, spanning $\sim 95\%$ of the age of the Universe.

AGN clustering is a reflection of the dark matter halos in which these objects are embedded. LSST's enormous dynamic range in luminosity and redshift will place important constraints on models for the relationship between AGN and the dark matter distribution, as described in § 10.3. LSST will significantly increase the number of high-redshift quasars, where the average co-moving separation of currently known luminous quasars is as high as 150 h^{-1} Mpc (at $z \sim 4$) — so sparse as to severely limit the kinds of clustering analyses that be can done, hindering our ability to distinguish between different prescriptions for AGN feedback.

AGN are an inherently broad-band phenomenon with emission from the highest-energy gamma-rays to long-wavelength radio probing different aspects of the physics of the central engine. LSST will overlap surveys carried out in a broad range of wavelengths, allowing studies of a large number of multi-wavelength phenomena (§ 10.4). LSST's multiwavelength power comes from the ability to compare with both wide-area and "pencil-beam" surveys at other wavelengths. The former are important for investigations of "rare" objects, while the latter probe intrinsically more numerous, but undersampled populations.

In all, the LSST AGN survey will produce a high-purity sample of at least ten million well-defined, optically-selected AGNs (§ 10.1). Utilizing the large sky coverage, depth, the six filters extending to 1μm, and the valuable temporal information of LSST, this AGN survey will dwarf the largest current AGN samples by more than an order of magnitude. Each region of the LSST sky will receive roughly 1000 visits over the decade-long survey, about 200 in each band, allowing variability to be explored on timescales from minutes to a decade, and enabling unique explorations of central engine physics (§ 10.5).

The enormous LSST AGN sample will enable the discovery of extremely rare events, such as transient fueling events from stars tidally disrupted in the gravitational field of the central SMBH (§ 10.6) and large numbers of multiply-lensed AGN (§ 10.7). Lastly, the giant black holes that power AGN inspire strong interest among students and the general public, providing natural avenues for education and public outreach (§ 10.8).

10.1 AGN Selection and Census

Scott F. Anderson, Xiaohui Fan, Richard F. Green, Gordon T. Richards, Donald P. Schneider, Ohad Shemmer, Michael A. Strauss, Daniel Vanden Berk

10.1.1 AGN Selection

There are three principal ways in which AGN will be identified in LSST data: from their colors in the LSST six-band filter system, from their variability, and from matches with data at other wavelengths.

Color Selection

Unobscured AGN with a broad range of redshifts can be isolated in well-defined regions of optical–near-IR multicolor space (Fan 1999; Richards et al. 2001). At low redshifts ($z \lesssim 2.5$), quasars are blue in $u-g$ and $g-r$ (these are the ultraviolet excess sources of Sandage 1965 and Schmidt & Green 1983), and are well-separated from stars in color-color space. At higher redshift, the Ly-α forest (starting at 1216Å) and the Lyman limit (at 912Å) march to ever longer wavelengths, making objects successively redder.

Figure 10.1 shows the colors of quasars and stars as convolved with the LSST filters, with data taken from the SDSS. The u-band data are crucial for selection of low-redshift ($z < 2$) AGN; observations in this filter allow one to distinguish between AGN and stars (in particular white dwarfs and A and B stars). High-redshift AGN will be easily distinguished; as we discuss in more detail below, the y filter should allow quasars with redshifts of 7.5 to be selected (compare SDSS, whose filter set ends with the z band; it has discovered quasars with redshift up to 6.4, Fan et al. 2006a). As with SDSS, most of the sample contamination is in the range $2.5 < z < 3$, where quasar colors overlap the stellar locus in most projections. It is also difficult to select quasars at $z \sim 3.5$, where Lyman-limit systems cause quasars to be invisible in u and g but quasars have similar colors to hot stars at longer wavelengths. However, lack of proper motion and variability will allow quasars to be efficiently separated from stars in these redshift ranges, as we describe below.

AGN color selection will proceed in much the same manner as for the SDSS; however, LSST's increased depth and novel observing strategy require consideration of the following issues:

- LSST (unlike SDSS) will not measure a given area of sky through the various filters simultaneously. Because of variability, the colors measured will, therefore, not exactly reflect the colors of the object at a given moment in time. However, the large number of epochs in each bandpass mean that the *average* colors of objects will be exactly what they would have been if the observations in each bandpass were simultaneous.
- For low-luminosity systems, the colors of AGN will be contaminated by the colors of their hosts. Simulated LSST images (e.g., § 3.3) will help to characterize this effect. Variability will allow objects with appreciable host-galaxy contribution to be selected, as will photometric measurements of unresolved point sources in the centers of galaxies.
- The majority of quasars used in Figure 10.1 are not significantly reddened. However, there is great interest in the reddened population (Richards et al. 2003; Maddox et al. 2008). While the most heavily obscured ("type 2") quasars will not be recognized as AGNs using LSST alone, LSST will detect millions of type 2 quasars via emission from their host galaxies and narrow-line regions. These objects can be recognized as AGNs by their infrared, radio, or X-ray emission, as we describe below.

Selection by Lack of Proper Motion

Lack of proper motion will further distinguish faint quasars from stars. The 3σ upper limit on proper motion for the full 10 years of the LSST survey is intended to be 3 milli-arcsec at $r \sim 24$, and five times better at $r = 21$. The stringent upper limit on proper motions will essentially eliminate the relatively nearby L and T dwarfs as contaminants of the very high-redshift quasar candidate lists, and will also remove many of the white dwarfs and subdwarfs.

It is illustrative to consider the case of contamination of the color selection by white dwarfs, which can overlap as ultraviolet excess objects at low redshift, and (for cooler white dwarfs) as objects with similar colors to $3.2 < z < 4.0$ quasars. For each quasar redshift, we use the white dwarf color-absolute magnitude diagram to estimate the white dwarf properties most closely matched to the quasar energy distribution as Holberg & Bergeron (2006). The typical distances of these objects at $r = 24$ place these contaminants in the thick disk population.

The width of the distribution of the thick disk component of the velocity dispersion is $\sim 60\,\mathrm{km\ s^{-1}}$ (Beers & Sommer-Larsen 1995). With a Gaussian form for the velocity dispersion and the 3σ upper limits for proper motion quoted above, we compute the fraction of the thick disk white dwarfs excluded.

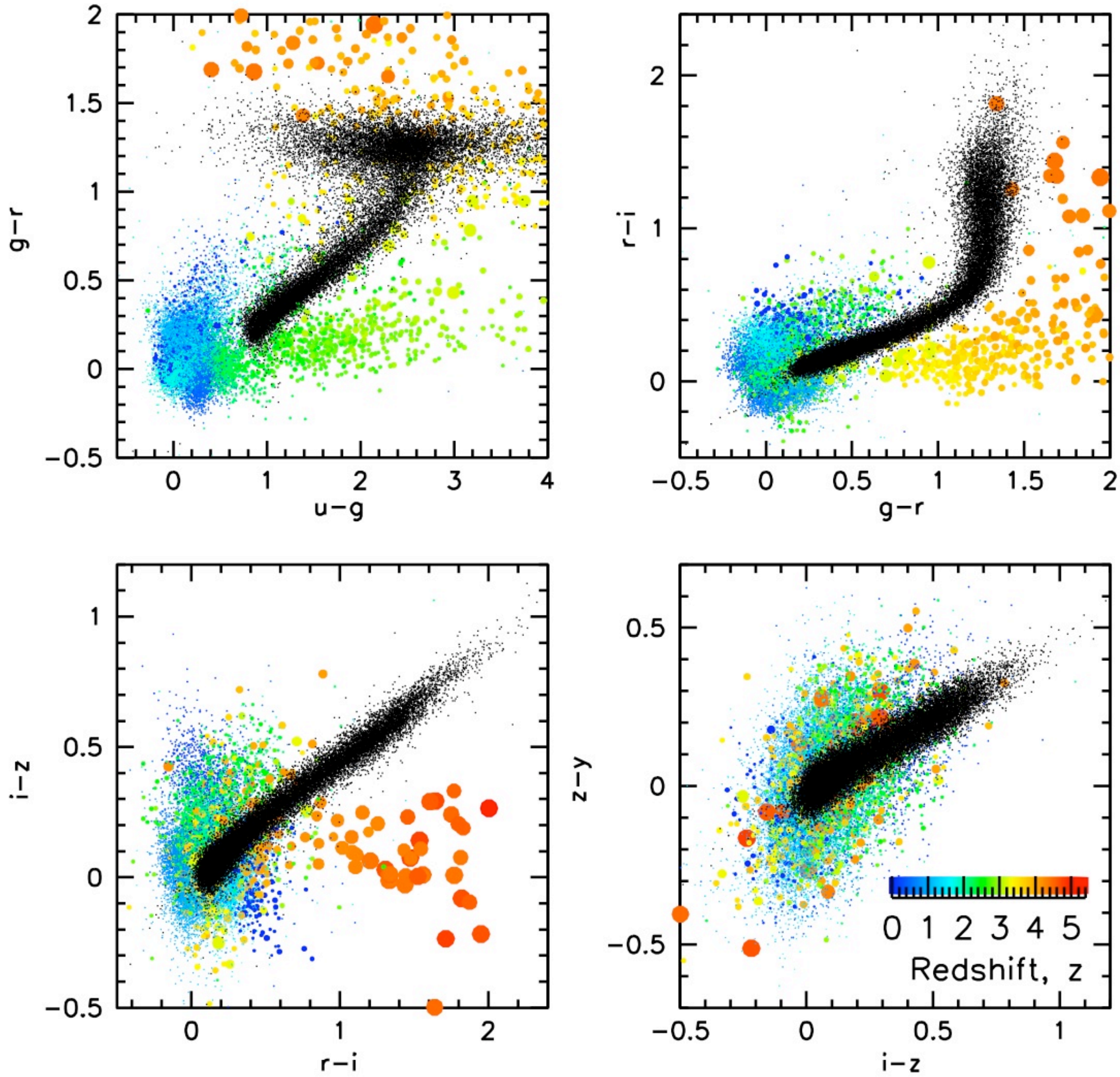

Figure 10.1: Color-color plots of known quasars from SDSS (colored dots) and stars (black dots) in the LSST photometric system. The quasars are color coded by redshift according to the color key, and for clarity, the dot size is inversely proportional to the expected surface density as a function of redshift. Since there is no y filter in the SDSS system, a random Gaussian color offset has been added to the $z-y$ color according to the width of the stellar locus in the $i-z$ color. The quasar colors become degenerate with those of F stars at redshifts between about 2.5 and 3. See Figure 10.5 and Figure 10.6 for redshifts above 5.

Table 10.1: Elimination of White Dwarf Contaminants

Quasar z	WD M_V for quasars $(V-I)$	WD $T_{\rm eff}$	Distance (pc) at $r=24$	3σ limit v_{tan} km s^{-1}	Fraction excluded
3.2	13.7	6500	1260	17.6	77%
3.6	15.7	4500	660	9.4	88%
4.0	16.5	3500	500	7.1	92%

If we consider a halo subdwarf at the main sequence turn-off detected at $r = 24$, the distance is some 50 kpc. Even then, the proper motion upper limit rejects half of the tangential velocity distribution of the outer halo, with its dispersion of $\sim 130\,\mathrm{km\ s}^{-1}$.

The conclusion is, therefore, that moderate to low-temperature white dwarfs will be effectively screened. The space distributions of hotter white dwarfs and main sequence stars earlier than K spectral type place the vast majority of them in the brighter magnitude range typical of the current SDSS samples. They would, therefore, not be expected to be significant contaminants at these faint magnitudes. An increasing fraction of the halo subdwarfs will remain as contaminants as the LSST survey limits are approached. The surface density of very distant halo main sequence stars is lower, which will minimize the contamination due to the poorer proper motion measurements at the faintest survey magnitudes.

Selection by Variability

Variability will add a powerful dimension to AGN selection by LSST, since AGN vary in brightness at optical and ultraviolet wavelengths with a red-noise power spectrum. It is expected that the efficiency of AGN selection by variability may be comparable to the color selection efficiency (Sesar et al. 2007). The amplitude of AGN variability depends upon rest-frame variability timescale, wavelength, luminosity, and possibly redshift (e.g., Vanden Berk et al. 2004). We use the parametrized description of AGN variability from the SDSS (Ivezić et al. 2004), extrapolated to fainter apparent magnitudes, to estimate the fraction of AGN in the LSST that may be detected as significantly variable. Given the depth of individual LSST exposures, we calculate the magnitude difference at which only 1% of the non-variable stars will be flagged as variable candidates due to measurement uncertainty, first assuming two measurement epochs separated by a month, and also assuming 12 measurement epochs spanning a year in total.

The probability that the single-band rms magnitude difference of an AGN will exceed this value, and will, therefore, be flagged as a variable candidate, depends upon redshift (as it determines rest wavelength and rest-frame variability timescale), luminosity, observed temporal baseline, and the number of observing epochs. Here we follow the model of Ivezić et al. (2004), and show the results in Figure 10.2.

Even with only two epochs separated by 30 days, a large fraction of AGN will be detected as variable objects. The fraction of AGN detected depends strongly on absolute magnitude at each redshift; intervening Lyman series absorption shortward of the 1216Å Lyman α emission line also affects the detection probability. After 12 epochs with a total temporal baseline of 360 days, nearly

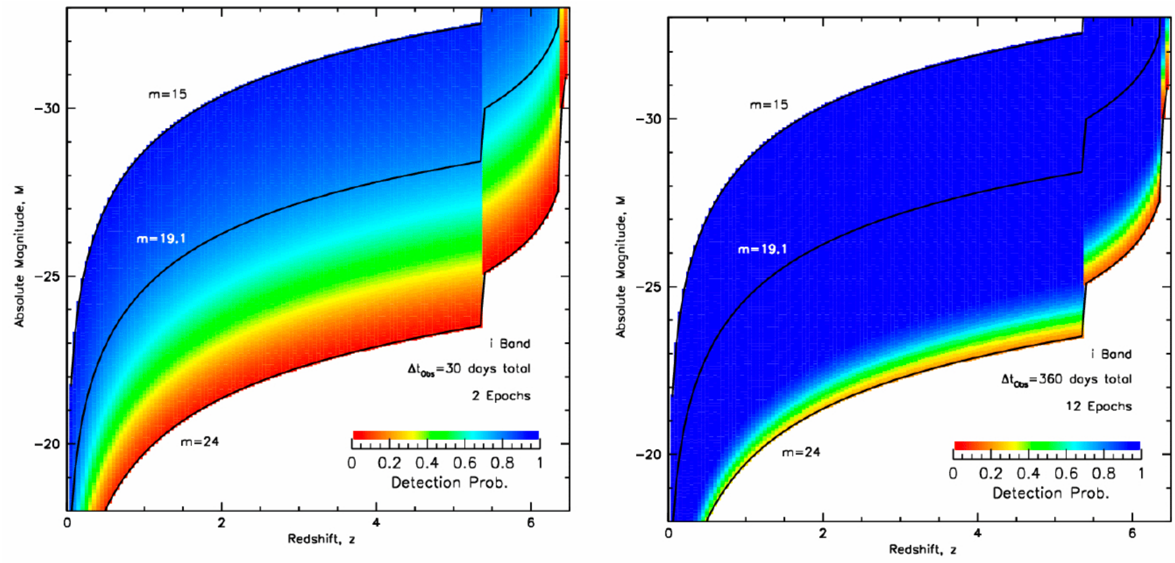

Figure 10.2: The probability of detecting an AGN as variable as a function of redshift and absolute magnitude. *Left:* two epochs separated by 30 days. *Right:* 12 epochs spanning a total of 360 days. Nearly all of the AGN between the limiting apparent magnitudes would be detected as variable after one year.

all of the AGN to a limiting apparent magnitude of 24 will be detected as variable. The detection fraction will increase as the number of epochs increases, and the use of all six bands will improve the detection fraction even further. Ultimately, LSST will provide $\sim$ 200 epochs for each AGN candidate in each band, thus increasing the detection fraction as well as increasing the limiting magnitude.

The LSST temporal information will be especially useful for selecting low-luminosity AGN which would otherwise be swamped by their hosts, as well as radio-loud AGN, which have larger variability amplitudes and shorter variability timescales (e.g., Giveon et al. 1999). Variability will also allow selection of AGN which are confused with stars of similar color, particularly at $z \sim 2.7$ where SDSS is highly incomplete. Variability timescales, coupled with LSST's 6-band photometry will allow clean separation of AGNs from variable stars. For example, RR Lyrae stars have similar colors to AGNs but have very different variability timescales (Ivezić et al. 2003), and can thus efficiently be identified as contaminants.

Selection by Combination with Multiwavelength Surveys

Cross-correlation of LSST imaging with multi-mission, multiwavelength surveys will also contribute to the AGN census by allowing selection of sources, such as optically obscured quasars, that cannot easily be identified as AGN by color selection, lack of proper motion, or variability. LSST's "deep-wide" nature will allow it to be combined both with shallower all-sky surveys at other wavelengths in addition to having both the areal coverage and depth to be paired with the growing number of multi-wavelength pencil beam surveys. For example, cross-correlations of LSST images with Chandra or XMM-Newton observations can reveal obscured AGN that are not easily identifiable via standard optical techniques; X-ray sources that have no LSST counterparts in any band may be

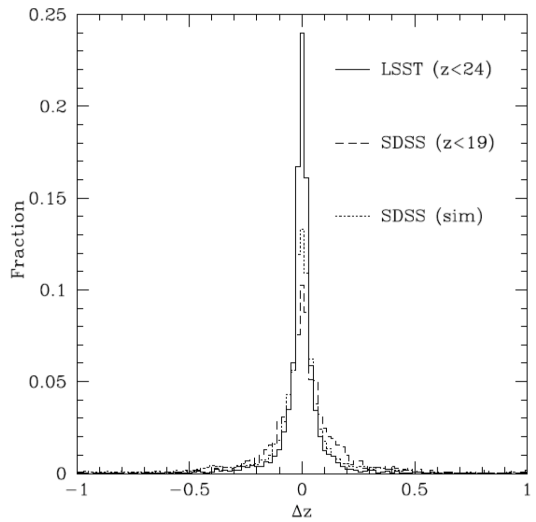

Figure 10.3: Distribution of the difference between photometric and spectroscopic redshifts ($\Delta z = z_{\rm spec} - z_{\rm phot}$) for UV-excess ($z \leq 2.2$) quasars (at higher redshifts, the sharp discontinuity in the spectral energy distribution (SED) caused by the onset of the Lyα forest is measureable by the LSST filter set, making photometric redshifts quite accurate). Results for known SDSS quasars to $i = 19.1$ (*dashed*) are compared with expected results from LSST to $r \sim 26.5$ (*solid*). LSST results assume the full 10-year co-added photometry. The simulated LSST quasar colors follow Fan (1999) (see also Richards et al. 2006a), using a distribution of power-law colors modulated by broad emission line features and inter-galactic hydrogen absorption. Photometric redshifts were determined using the algorithm of Weinstein et al. (2004). The dotted line shows the results from *simulated* SDSS quasars; they do better than the real data because of the limitations of our simulations. LSST's deeper imaging will allow accurate photometric redshifts to much fainter magnitudes than SDSS, while the addition of the y bandpass reduces the overall scatter.

candidates of $z > 7.5$ quasars. Many high-redshift AGN may also be detected by matching LSST images with a growing array of future multi-wavelength surveys; see § 10.4 for further discussion.

10.1.2 Photometric Redshifts

As LSST is a purely photometric survey and AGN science generally requires having accurate redshifts, photometric redshift determinations are a crucial part of the project. To zeroth order, the continuum of an unobscured quasar longward of Lyα is a power-law, and thus its colors are independent of redshift. However, the broad strong emission lines of high equivalent width modulate the colors as a function of redshift, allowing photometric redshifts to be determined with surprising fidelity (Weinstein et al. 2004; Richards et al. 2009), especially once the Lyα forest enters the filter set. SDSS was able to determine photometric redshifts for quasars to $\Delta z = \pm 0.3$ for 80% of SDSS quasars ($i \sim 19$; Richards et al. 2009). Even without the y-band LSST will do at least that well to $i \sim 24$.

Figure 10.3 shows that for UV-excess quasars, LSST will produce considerably more precise photometric redshifts, with more than 80% of quasars having photometric redshifts accurate to $\Delta z = \pm 0.1$ (SDSS did this well for only 60% of quasars). With LSST's exquisite astrometry (§ 6.12), the subtle effects of emission lines on chromatic aberration will be measureable, allowing an independent estimate of redshift (Kaczmarczik et al. 2009). When combined with photometric redshifts, we estimate that the fraction of quasars with redshifts correct to $\Delta z = \pm 0.1$ will be of order 90%.

10.1.3 Expected Number of AGN

The growth in the benchmark sizes of individual quasar samples is impressive over the past several decades, starting at $N \sim 10^{0-1}$ (e.g., Schmidt 1963, 1968), but growing rapidly to 10^2 (e.g., Braccesi et al. 1970; Schmidt & Green 1983), and then to $N \sim 10^3$ (e.g., Hewett et al. 1993) by the 1990s. The most recent decade has seen the continuation of an exponential expansion in the number of quasars identified in homogeneously selected samples, extending to moderate depth: 25,000 color-selected quasars to $b_J < 20.85$ are included in the final 2dF QSO Redshift Survey catalog (Croom et al. 2004), and SDSS is approaching $N \sim 10^5$ spectroscopic quasars (mostly with $i < 19.1$) (Schneider et al. 2007), and $N \sim 10^6$ photometrically-selected quasars to $i < 21.3$ (Richards et al. 2009). LSST will provide a major leap forward in quasar sample size, plausibly identifying over 10^7 quasars to beyond $m \sim 24$ through the variety of selection approaches we've just outlined.

An estimate of LSST's coverage of the quasar redshift-magnitude plane is given in Table 10.2. The numbers of quasars in the various bins were calculated using the quasar luminosity function of Hopkins et al. (2007b), extrapolated to low luminosities. Hopkins et al. (2007b) combines the most recent measurements of the luminosity function from optical, IR, and X-ray data to provide the most robust determination available to date of the *bolometric* luminosity function over the redshift and luminosity ranges that LSST will survey. These results are in good agreement with those of the 2dF SDSS Luminous Red Galaxy and Quasar Survey data (Croom et al. 2009b), which is restricted to lower redshift and lower luminosity than LSST will probe. In all, LSST will detect over 10 million type 1 AGN with $M_i \leq -20$, $i \leq 24.5$ and redshifts below 6.5; this number rises to as many as 16 million for $i \leq 26.25$.

At very high redshift ($z > 6$) and faint luminosities, a better estimate is provided by the Fan et al. (2006b) and Jiang et al. (2009) samples. Predictions for $z > 6$ quasars from these studies are shown in Figure 10.4. LSST can detect significant number of quasars up to $z \sim 7.5$, after which quasars become y drop-outs. Indeed, one of the most important discoveries of LSST is expected to be the detection of many AGN at the end of the cosmic "Dark Ages." Figure 10.6 shows that the y-band filter will permit selection of quasars out to $z \sim 7.5$ and down to moderate AGN luminosities ($\approx 10^{45}$ ergs s^{-1}) in impressively high numbers due to the steepness of the luminosity function at high redshifts. Such quasars should be detected as z-band dropouts and will be followed up spectroscopically from the ground and with JWST. This will exceed the current number of the most distant SDSS quasars at $5.7 < z < 6.4$ by an order of magnitude (e.g., Fan et al. 2006a). The LSST census of $z \sim 7$ quasars will place tight constraints on the cosmic environment at the end of the reionization epoch and on the SMBH accretion history in the Universe.

The Chandra Deep Fields show a surface density of order 7000 AGN per deg^2 (e.g., Bauer et al. 2004; Brandt & Hasinger 2005), which, when extrapolated to the 20,000 deg^2 of LSST, implies a total count of over 10^8 AGN, an order of magnitude larger than the optical AGN luminosity function would predict. This may be thought of as a reasonable upper limit to the number of AGN that LSST might find, as it includes optically obscured objects and may include objects of intrinsically

i	0.5	1.5	2.5	3.5	4.5	5.5	6.5	Total
16	666	597	254	36	0	0	0	1550
17	4140	4630	1850	400	54	0	0	11100
18	19600	28600	10700	1980	321	19	0	61200
19	68200	131000	53600	8760	1230	115	0	263000
20	162000	372000	194000	35000	4290	441	1	767000
21	275000	693000	453000	113000	14000	1380	34	1550000
22	336000	1040000	756000	269000	41200	3990	157	2450000
23	193000	1440000	1060000	476000	103000	10900	527	3280000
24	0	1370000	1360000	687000	205000	27400	1520	3660000
25	0	314000	1540000	888000	331000	60800	4100	3140000
26	0	0	279000	760000	358000	86800	7460	1490000
Total	1060000	5390000	5720000	3240000	1060000	192000	13800	16700000

Table 10.2: Predicted Number of AGN in 20,000 deg^2 over $15.7 < i < 26.3$ and $0.3 < z < 6.7$ with $M_i \leq -20$. The ranges in each bin are $\Delta i = 1$ and $\Delta z_{em} = 1$, except in the first and last bins where they are 0.8 and 0.7, respectively.

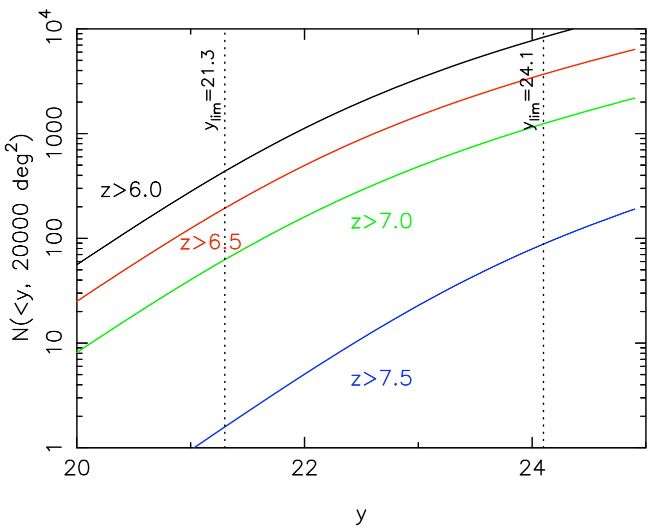

Figure 10.4: Number of high-redshift ($z > 6$) quasars expected to be discovered in a 20,000 deg^2 area as a function of redshift and limiting magnitude. We use the luminosity function (LF) at $z \sim 6$ measured by Jiang et al. (2009). We assume that the density of quasars declines with redshift as measured in Fan et al. (2001, 2006a) and continues to $z > 6$, with the same LF shape. Two vertical dashed lines indicate the 10-σ detection limit for LSST for a single visit and for the final coadd.

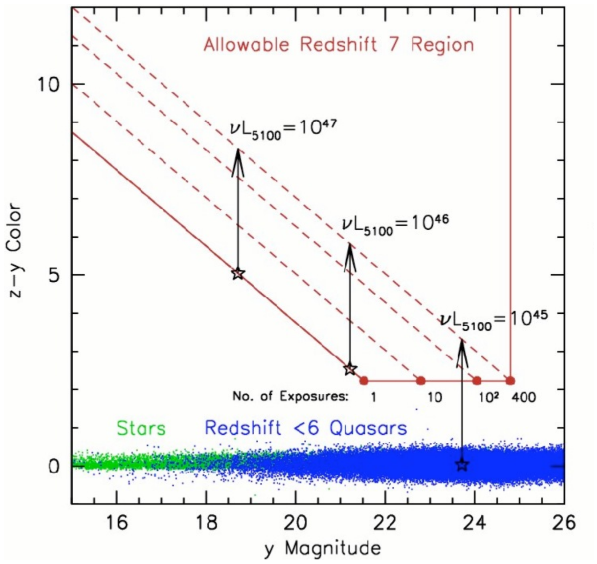

Figure 10.5: LSST $z - y$ vs. y color-magnitude diagram, showing the expected region in which $z \sim 7$ quasar candidates will lie. The region limits are defined by the 5 σ y-magnitude detection limits, and 2 σ z-magnitude detection limits, as a function of the number of co-added 15 s exposures. An object is considered a $z \sim 7$ candidate if it is detected at the $> 5\ \sigma$ level in the y-band, and does not exceed the z band 2 σ detection limit. The y-magnitudes and $z - y$ color limits are shown for simulated $z = 7$ quasars at three different 5100 Å continuum luminosities. The open stars show the minimum $z - y$ color limits required for a single 15 s exposure, and the ends of the arrows show the limits for 400 exposures (the full extent of the 10-year survey). The expected $z - y$ colors of stars (green) and $z < 6$ quasars (blue), based on results from the SDSS, are shown for comparison.

lower luminosity than we have assumed, and may also point to errors in our extrapolation of the measured luminosity function. Indeed, this gives us motivation to *measure* the luminosity function, as we discuss below in § 10.2.

10.2 AGN Luminosity Function

Scott F. Anderson, Richard F. Green, Gordon T. Richards, Donald P. Schneider, Ohad Shemmer

The census of AGN through cosmic time, tracing the evolution of supermassive black holes, may be quantified via the AGN luminosity function (hereafter, LF), as well as closely related empirical measures such as the $\log N - \log S$ curve. The LF impacts studies of the ionizing background radiation, the X-ray background, and quasar lensing, and constrains a variety of parameters in physical models for the evolution of AGNs, including black hole masses, accretion rates and Eddington ratios, the fraction of massive galaxies (perhaps most) that undergo an AGN phase and the lifetime of this phase, and cosmic down-sizing (e.g., Kauffmann & Haehnelt 2000; Wyithe & Loeb 2002; Hopkins et al. 2007b). The variety and sensitivity of LSST-enabled, AGN-selection metrics will result in a high-quality, representative AGN sample required for detailed LF studies. In particular, the large area, depth, and dynamic range of LSST form a superb basis to study the populous faint end of the LF at moderate to high redshifts.

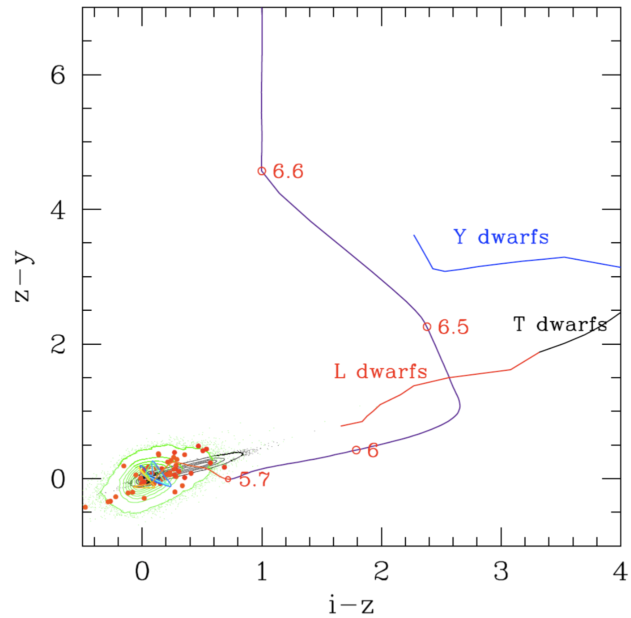

Figure 10.6: Distribution of objects in $i-z, z-y$ color space. Ordinary stars are shown as the black contours, while low-redshift quasars are the green contours; those quasars with redshift above 5 are red dots. The loci show the expected tracks of higher-redshift quasars (with redshifts labeled), and brown dwarfs of type L, T, and Y, as labelled.

While there has been exponential growth in quasar survey samples in the last few decades (§ 10.1.3), there has been far less progress at "ultrafaint" ($m > 22.5$) magnitudes that sample the low-luminosity end of the LF. For example, the pioneering photographic studies of Koo, Kron, and collaborators (e.g., Koo et al. 1986) which extend to $B < 22.6$ over 0.3 deg^2, are still often quoted in current studies as among the handful of reliable points in LF studies of the faint AGN population. Significant expansions in areal coverage from a few $m \sim 22.5$ modern CCD-based surveys are underway (e.g., 3.9 deg^2 in the SDSS faint quasar survey of Jiang et al. 2006).

Yet there are strong motivations in LF studies to explore much fainter than the break in the number counts distribution, and this sparsely sampled ultrafaint regime is one where LSST is poised to have significant impact on LF studies. Only ultrafaint ($m > 22.5$) surveys can probe the populous, faint end of the AGN LF, especially at moderate to high redshifts. For example, an AGN with absolute magnitude $M = -23$, i.e., a high space density object from the faint end of the luminosity function, will have apparent magnitude $m > 22.5$ at $z > 2.1$.

Figure 10.7 shows our current understanding of the optical AGN counts as a function of magnitude. Among the most reliable points well beyond $m > 22.5$ are those of the Wolf et al. (2003) COMBO-17 survey, although there are a handful of other smaller area optical surveys using a variety of selection criteria that give similar results at least for AGNs out to $z < 2.1$. This figure suggests that LSST will discover on the order of 500 photometric AGNs/deg^2 to $m < 24.5$ and $z < 2.1$, in rough agreement with the numbers we found above. To the extent that we can identify AGNs from the co-added data below the single-visit limits, we should be able to find appreciably more objects.

Given the very large numbers of AGNs that LSST will find, a bin of a few tenths in redshift

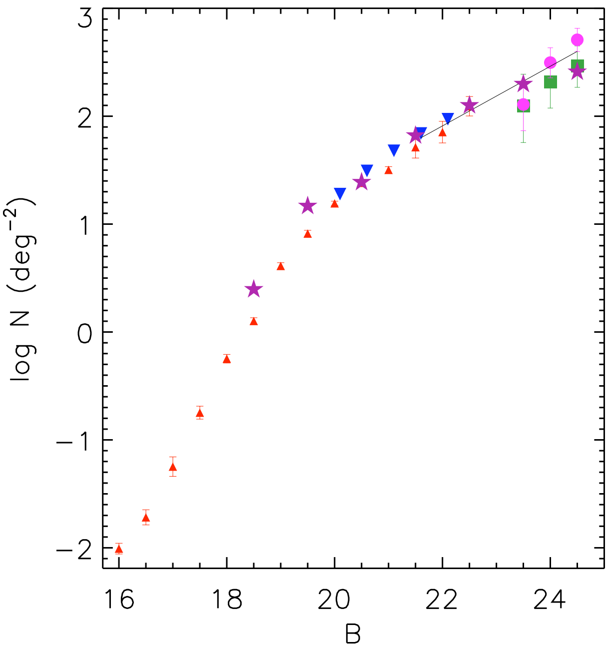

Figure 10.7: A summary of our current understanding of the numbers of AGNs per square degree of sky brighter than a given apparent magnitude, adapted from Beck-Winchatz & Anderson (2007). The ultrafaint points are from the COMBO-17 survey (purple stars; Wolf et al. 2003) and HST based surveys (pink circles and green squares; Beck-Winchatz & Anderson 2007). Shown for broad comparison are: brighter 2SLAQ points (blue, upside-down triangles; Richards et al. 2005); a simple extrapolation of 2SLAQ points to ultrafaint magnitudes (solid line); and the Hartwick & Schade (1990) compilation (small, red triangles), which incorporates many earlier quasar surveys. The data show ~ 500 AGNs deg^{-2} to $m < 24.5$ and $z < 2.1$. The LSST AGN surveys will extend both fainter and across a much wider redshift range, suggesting a sample of at least $\sim 10^7$ AGNs.

covering a decade in luminosity will include thousands of AGNs over much of the redshift range, allowing statistical errors to be negligible, and systematic errors (due to errors in photometric redshifts, bolometric corrections, or selection efficiency) will dominate our measurements. Of course the efficacy of any AGN census for establishing the LF is not measured merely by the numbers of objects sampled. Survey depth, sky coverage, dynamic range, completeness, contamination, redshift range, and wavelength selection biases/limitations, are all additional key elements. As an example, a recent survey embodying many of these as attributes is the 2SLAQ survey of 8700 AGNs over 190 deg^2, which extends to $g < 21.85$ (Croom et al. 2009a). But the dynamic range, redshift range, depth, and sky coverage of the LSST AGN sample will be much more impressive.

The impact of LSST depth and dynamic range in magnitude and redshift for ultrafaint AGN LF studies may be seen in the context of current LF models. One popular form for the LF considered in many recent studies is a double power law with characteristic break at luminosity L_*. The LF shape might evolve with redshift in either luminosity, density, or both (e.g., Schmidt & Green 1983). For several decades, studies tended to favor pure luminosity evolution models, but some recent studies from various wavebands (some extending quite deep in small areas, such as the X-ray studies of Ueda et al. 2003; Hasinger et al. 2005) have found markedly disparate evolutionary rates, depending on their energy selection wavebands. Preliminary indications are that the slope of the AGN luminosity function varies considerably from $z = 2$ to $z = 6$ (Richards et al. 2006b; Jiang et al. 2008). In reconciling multiple survey results from various wavebands, there has been a recent resurgence in combined luminosity/density evolution models (e.g., Schmidt & Green 1983; Hasinger et al. 2005; Croom et al. 2009a), which incorporate "cosmic downsizing" (Cowie et al. 1996) scenarios for the LF. These are well represented by the bolometric LF studies of Hopkins et al. (2007b), who argue that the peak of the AGN space density occurs at increasing redshifts for more luminous AGNs (see also Croom et al. 2009b).

In the currently popular merger plus feedback model of Hopkins et al. (2006), the faint-end slope of the luminosity function is a measure of how much time quasars spend accreting at sub-Eddington rates (either before or after a maximally accreting state). The bright-end slope, on the other hand, tells us about the intrinsic properties of quasar hosts (such as merger rates). If these two slopes are fixed with cosmic time, then the space density of AGN will peak at the same redshift at all luminosities — contrary to recent results demonstrating downsizing, whereby less luminous AGNs peak at lower redshift as the average mass of accreting supermassive black holes moves to lower scales with cosmic time. Thus, understanding the evolution of the bright- and faint-end quasar LF slopes is central to understanding cosmic downsizing.

Figure 10.8 (adapted from figure 8 of Hopkins et al. 2007b) shows a realization of one of these downsizing models: it adopts the usual double power-law shape, but allows for a break luminosity L_* that evolves with redshift, as shown by the solid line. Superposed are dotted red curves representative of the faint limits of the 2SLAQ and the SDSS photometric surveys (Richards et al. 2005, 2009). These surveys, however, don't probe significantly beyond the break luminosity for redshifts much larger than 2. The bright limit is indicated by the cyan curve, and the faint limit in a single visit probes to the break luminosity to $z = 4.5$, and to $z = 5.5$ in the co-added images, even in this model in which the break luminosity decreases rapidly at high redshift. Thus the LSST-determined quasar LF will provide crucial insights to our understanding of AGN feedback in the early Universe and how it influences the evolution of massive galaxies.

With the large number of objects in the sample, the dominant uncertainties in LF studies will be systematics, such as the contamination of the sample by non-AGNs, completeness, and uncertainties associated with photometric redshifts. Internal comparison of LSST color-, variability-, and proper motion-selected AGN surveys will limit contamination and enhance completeness (§ 10.1.1), while comparison with deep Chandra X-ray and Spitzer mid-IR data will allow the selection effects to be quantified. There is clearly a need as well for spectroscopic follow-up of a modest subset of the full LSST sample to further quantify the contamination of the sample from non-AGN.

10.3 The Clustering of Active Galactic Nuclei

Michael A. Strauss, Robert J. Brunner, Jeffrey A. Newman

One way that we can get a handle on the physical nature of the galaxies that host AGN and the conditions that cause infall and growth of the black hole is to study the spatial clustering of the AGN. The relationship between AGN clustering and that of "ordinary" galaxies can give important clues about how the two are physically related.

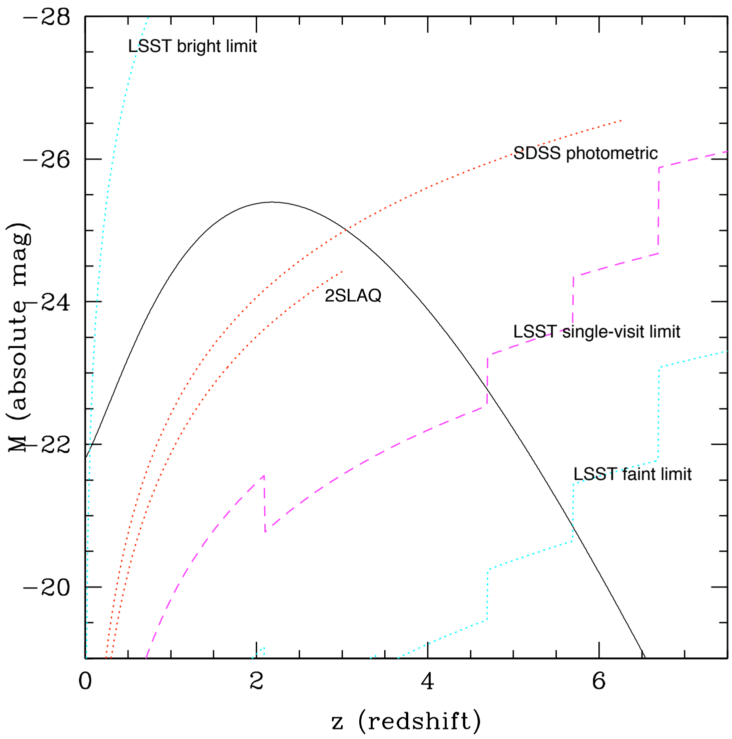

Figure 10.8: Depth and redshift coverage of large, optical surveys, compared to a representation of the LF of Hopkins et al. (2007b). The evolution of the break luminosity L_* with redshift is shown by the solid black curve (adapted from Hopkins et al.). The corresponding sensitivity of two current large quasar surveys is depicted by the dotted red curves (2SLAQ and SDSS photometric surveys; Richards et al. 2005, 2009). The depth of the LSST AGN survey will permit a much more sensitive measure of the break luminosity evolution at intermediate to high redshifts, encompassing (in a single sample) $0 < z < 4.5$ (magenta curve reflecting LSST single-visit depth), and perhaps $0 < z < 5.5$ (lower cyan curve reflecting final, stacked LSST depth). The cyan curve to the upper left reflects the bright limit of LSST (in a single visit).

The luminous parts of galaxies of course represent only a small fraction of the clustered mass density of the Universe, and there is no guarantee that the clustering apparent from the matter that we see matches that of the underlying dark matter perfectly (§ 9.5). A common hypothesis, which is predicted, e.g., in so-called *threshold bias* models in which galaxies form only in regions of high density contrast in the dark matter, is that the fractional density contrast $\delta(\mathbf{r}) \equiv \frac{\rho(\mathbf{r})-\langle\rho\rangle}{\langle\rho\rangle}$ as measured for galaxies is proportional to that of the dark matter:

$$\delta_{galaxies} = b\,\delta_{dark\ matter}.$$

Here where the bias factor b may be a function of the smoothing scale on which ρ is measured. This simple relation is often referred to as a linear bias model (as opposed to models which include higher-order terms or scatter around this simple deterministic relation; see also the discussion of halo occupation distribution models in § 9.4 and § 9.5.4).

In threshold bias models, the bias factor b is directly related to the value of the threshold. Thus one can determine the characteristic mass of the dark matter halos associated with a given sample of galaxies directly from a measurement of their clustering. The higher the halo mass associated with the galaxy population in question, the higher the bias, and, therefore, the stronger the expected clustering.

In practice, clustering is quantified by measuring the correlation function $\xi(r)$ (or its Fourier Transform, the power spectrum) of the galaxy sample, as described in § 9.5.4, and comparing it with that of the underlying dark matter as predicted from linear theory (on large scales) or N-body simulations (on smaller, non-linear scales). The linear bias model states

$$\xi_{galaxies} = b^2 \xi_{dark\ matter}, \tag{10.1}$$

where again b may be a function of scale. Our current cosmological model is precise enough to allow a detailed prediction for $\xi_{dark\ matter}$ to be made.

The galaxy correlation function at low redshift has been measured precisely, using samples of hundreds of thousands of galaxies (from the redshift survey of the SDSS; see, e.g., Zehavi et al. 2005; Eisenstein et al. 2005), allowing quite accurate determination of the bias as a function of scale for various subsets of galaxies. However, AGN are rarer, and the measurements are not as accurate (for example, the mean separation between $z \sim 3$ quasars in the SDSS is of order 150 co-moving Mpc). The enormous AGN samples selectable from LSST data (§ 10.1) will cover a very large range of luminosity at each redshift, allowing the clustering, and thus bias and host galaxy halo mass, to be determined over a large range of cosmic epoch and black hole accretion rate.

While gravitational instability causes the contrast and, therefore, the clustering of dark matter to grow monotonically with time, observations of galaxies as a function of redshift shows their clustering strength measured in co-moving units to be essentially independent of redshift (albeit with increasingly larger error bars at higher redshift). This is roughly as expected, if (for a given population of galaxies) the characteristic halo mass is independent of redshift. As one goes to higher redshift, and therefore further back in time, the amplitude of the underlying dark matter clustering decreases, meaning that this characteristic halo mass represents an ever-larger outlier from the density contrast distribution, and is therefore ever more biased. Quantifying this relation allows one to measure the characteristic halo mass of galaxies as a function of redshift (Ouchi et al. 2005).

We would like to do the same for AGN, to determine the masses of those halos that host them. The observed correlation function of luminous quasars at all redshifts below $z \sim 3$ is very similar to that of luminous red ellipticals, suggesting that they live in similar mass halos, and perhaps that these quasars are hosted by these elliptical galaxies (e.g., Ross et al. 2009, and references therein).

How does the clustering depend on AGN luminosity? The AGN luminosity depends on the mass of the central black hole, and the Eddington ratio. It has been suggested that the mass of the central black hole is correlated with that of its host halo at low redshift (Ferrarese 2002); after all, these black holes are correlated with the mass of the spheroidal components of galaxies, and the masses of these spheroids are plausibly correlated with the mass of the halo, as modern Halo Occupation Distribution (HOD) models would suggest. Thus if most AGN are accreting at close to the Eddington limit (Kollmeier et al. 2006; Shen et al. 2008a), one might imagine a fairly significant correlation of clustering strength with luminosity. If, on the other hand, luminosity is driven more by a range of Eddington ratios, such luminosity dependence becomes quite weak (Lidz et al. 2006). Models of black hole growth differ largely on questions of the duration of the accretion and the level and constancy of the Eddington ratio, thus measurements of the luminosity dependence of the clustering strength become particularly important.

Current samples, however, simply do not have the dynamic range in luminosity at any given redshift to allow this test to be done robustly. For example, the SDSS quasar sample (Richards et al. 2006b) has a range of only about two magnitudes (a factor of less than 10 in luminosity) over most of its redshift range. Samples going deeper do exist over small areas of sky, but do not probe the large scales where the linear clustering is best measured. The current measurements of the luminosity dependence are poor: the data are consistent with no luminosity dependence at all (although there is a hint of an upturn for the highest luminosity decile, Shen et al. 2008b), but the error bars are large, the range of luminosities tested is small, and redshift and luminosity evolution are difficult to separate out.

LSST will increase the dynamic range enormously over existing samples. At most redshifts, we will be able to select AGN with absolute magnitudes ranging from -29 to -20 (Table 10.2), a factor of several thousand in luminosity, and the numbers of objects in moderate luminosity bins will certainly be large enough to measure the correlations with high significance. There must be a luminosity dependence to the clustering at some level if black hole masses are at all correlated with halo masses; this may only become apparent with samples of such large dynamic range.

At higher redshifts, Shen et al. (2007) have found that the clustering length grows with redshift: $17 \pm 2\,h^{-1}$Mpc at $z \sim 3.2$, and $23 \pm 3\,h^{-1}$Mpc at $z \sim 4$; (Shen et al. 2007). This suggests both that the most luminous objects at these redshifts are accreting at close to the Eddington limit (and, therefore, their luminosities reflect their black hole masses), *and* the black hole masses are tightly coupled to their halo masses (White et al. 2008). Exploring these connections at lower luminosities is crucial, as has been emphasized by Hopkins et al. (2007a), where different models for AGN feeding can be distinguished by the luminosity dependence of clustering at $z > 3$. This is illustrated in Figure 10.9, which shows the substantial dependence of the quasar bias and co-moving clustering length on redshift and luminosity as predicted in various models. Most of the luminosity dependence, and the distinction between models, becomes apparent at $z > 3$, where existing data are very limited. Figure 10.10 shows both the angular quasar auto-correlation, and the quasar-galaxy cross-correlation, that we might expect for a sample of 250,000 quasars with $2.75 < z < 3.25$ with $g < 22.5$ (i.e., easily visible in a single visit). The error bars are calculated using the formalism of Bernstein (1994). In fact, our photometric redshifts will be good enough to explore clustering in substantially finer redshift bins, strengthening the clustering signal (§ 10.1.2). Even with broad redshift bins, correlation function errors are small enough that we can divide the sample into many bins in luminosity, color, or other properties, allowing us to explore both the redshift and luminosity dependence of the clustering strength. For cross-correlation studies, errors in the clustering measurements at small scales depend only weakly on sample size (as $1/sqrtN$), allowing $S/N > 10$ measurements even for samples 10 times smaller than the one shown here.

From the measurement of quasar clustering, we get an estimate of the minimum mass of the halos hosting them. Given a cosmological model, the number density of halos of that mass can be predicted, and the ratio to the observed number density of quasars allows inference of the duty cycles of quasars. With existing data (Shen et al. 2007), this test gives uncertainties of an order of magnitude; with LSST, this can be done much more precisely and explored as a function of luminosity, thereby further constraining models of AGN growth.

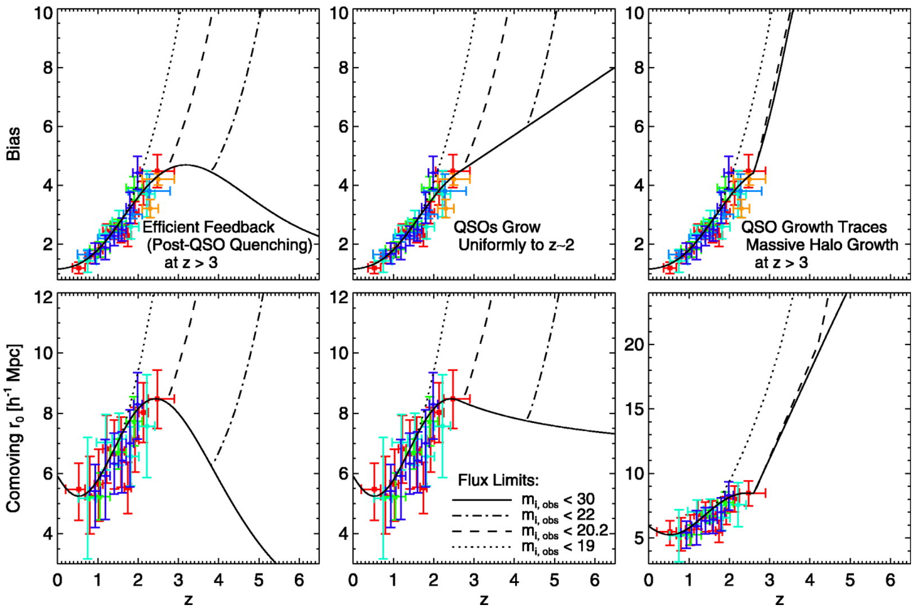

Figure 10.9: The bias (top panels) and comoving clustering length (lower panels) of quasars in three models of quasar growth, for samples of various limiting magnitude. LSST will be able to probe to limiting magnitudes of $m \sim 26$ reliably. Measured data points, entirely limited to $z < 2.5$, are shown as colored points with error bars. Note that the models are essentially entirely degenerate, with no luminosity dependence, in this redshift range; all the action is at $z > 3$. Even at $z > 3$, one needs to go appreciably fainter than the SDSS magnitude limit to break the degeneracy. The three models are (left to right): an efficient feedback model (in which infall to the SMBH halts immediately after a quasar episode); a model in which SMBHs grow smoothly to $z = 2$; and a model in which black hole growth is tied to that of the dark matter halo to $z = 2$. Figure from Hopkins et al. (2007a), with permission.

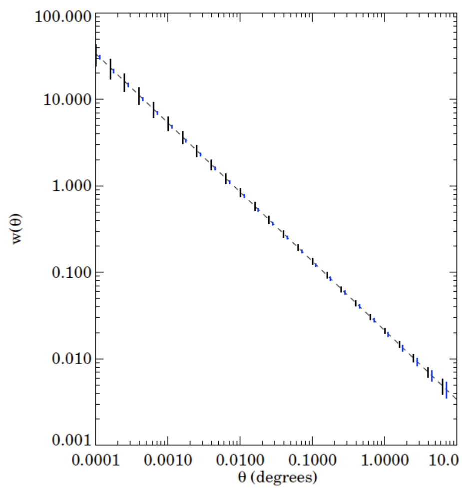

Figure 10.10: The predicted angular auto-correlation of quasars (black) and cross-correlation between quasars and galaxies (blue), for a sample of 250,000 quasars with $g < 22.5$ with redshifts between 2.75 and 3.25. The underlying three-dimensional auto- and cross-correlation functions are assumed for the purposes of the figure to be the same pure powerlaw, $\xi(r) = (r/10\,h^{-1}\mathrm{Mpc})^{-1.8}$ in co-moving coordinates. The galaxy sample extends to $i < 25$. The error bars are calculated using the formalism of Bernstein (1994). Even 10× smaller quasar samples will yield useful clustering measurements via cross-correlation techniques.

The small-scale clustering of AGN can be studied in great detail with LSST; the co-added photometry will go deep enough to see host clusters, for example, to at least $z = 4$. This gives an independent test of bias relations as a function of redshift; given that the highest-redshift quasars are so strongly biased, they live in particularly massive halos and, therefore, are likely to lie in regions in galaxy overdensity. These data will allow us to explore how quasars fit into the Halo Occupation Distribution picture as a function of luminosity and redshift (§ 9.4). Indeed, the quasar-galaxy cross-correlation function can be measured to much higher precision than the auto-correlation function, simply because there are so many more galaxies in the sample (see the discussion in § 9.5.4). As Padmanabhan et al. (2008) describe, the cross-correlation of quasars with either the general galaxy population or specific galaxy subsamples can be directly compared to the auto-correlation of that galaxy sample to place constraints on the quasar bias, its evolution with redshift and luminosity, and the quasar host halo mass at different cosmic epochs (Coil et al. 2007).

LSST will also be able to resolve close companion galaxies to quasars, allowing us explore how mergers drive quasar activity. Finally, the stacked images will go to low enough surface brightness and have enough dynamic range to separate out quasar host galaxy light; an important exercise for the future is to quantify to what extent this will be doable as a function of luminosity and redshift.

Finally, LSST will explore the nature of quasar pairs and the quasar correlation function on small (< 1 Mpc) scales. It is known that quasars show an excess of pairs over what is expected given an extrapolation of the power-law from larger scales (Djorgovski 1991; Hennawi et al. 2006; Myers et al. 2006). Is this excess due to triggering of quasar activity in dense environments? This will be explored with exquisite statistics and over a wide range of luminosity and redshift with LSST. Even projected pairs are tremendously useful; follow-up spectroscopy allows the environments (IGM, companion galaxies) and isotropy of the emission of the foreground object to be probed from their signature in the absorption spectra of the background object (Hennawi & Prochaska 2007).

10.4 Multi-wavelength AGN Physics

Scott F. Anderson, D.R. Ballantyne, Robert R. Gibson, Gordon T. Richards, Ohad Shemmer

AGN emit strongly across a very broad energy range, typically with prodigious luminosity spanning at least from the infrared through the X-ray, and sometimes extending to radio and/or gamma-ray energies as well. Although a power-law is often used to describe the broad underlying spectral energy distribution (SED) of AGNs, such a characterization is a marked oversimplification: quasars display a rich diversity of radiation emission and absorption features that add complexity to their SEDs, but also enable a more detailed understanding of their complicated, multi-region structure. In many cases, a specific structure — such as an accretion disk, a disk corona, a jet, or an outflowing wind — is primarily associated with emission or absorption in a particular energy band. A multi-wavelength view of AGN is needed to understand the total (bolometric) energy output of AGN, and also to study particular structures that may differ dramatically among AGN subclasses. For example, dust-obscured quasars are more readily found and studied in the infrared, and some quasar central engines enshrouded by moderately thick columns of intrinsic absorbing gas are best studied via hard X-rays.

Observations at other wavelengths are thus essential companions to LSST optical studies to obtain a reliable physical understanding of the structure of AGN, and to count and classify the wide range of observed multi-wavelength AGN phenomena with minimal bias. Moreover, the combination of multi-epoch LSST optical photometry with overlapping contemporaneous multiwavelength observations will provide unprecedented, time-dependent coverage of the AGN SED. Because LSST is repeatedly scanning a large portion of the sky, it will be possible to match LSST optical observations to any overlapping fields or individual AGN sources targeted contemporaneously by other missions, providing a near-simultaneous, multi-wavelength "snapshot" of the SED, as well as a description of the history and evolution of the source in LSST wavebands. Such time-dependent data will, for example, expand our knowledge of the co-evolution of accretion structures (e.g. Vanden Berk et al. 2004), and provide a unique view of remarkable sources such as blazars, highly-absorbed quasars, and perhaps new types of AGN that LSST will discover. LSST AGN studies will benefit from data taken with other telescopes or observatories of sources in the LSST sky, including upcoming or ongoing wide surveys such as VISTA (Sutherland 2009), WISE (Eisenhardt et al. 2009), EXIST (Grindlay 2009), JANUS (Burrows 2009), and Fermi (Michelson 2003), and existing wide surveys such as NVSS (Condon et al. 1998), SUMSS (Bock et al. 1999), 2MASS (Skrutskie et al. 2006), COSMOS (Scoville et al. 2007), GALEX (Martin et al. 2005), ROSAT (Truemper 1982), and XMM-Newton (Jansen et al. 2001).

10.4.1 Multi-wavelength AGN Classification

The depth and sky coverage provided by LSST are essential for characterizing and classifying optically faint AGN that are prominent in other wavebands, but that cannot be studied with shallower optical surveys such as the SDSS (York et al. 2000). Any sky areas—whether by design or by serendipity—in which past, present, or future deep multiwavelength surveys overlap with LSST sky coverage, will be promoted by LSST investigations to "optical plus multiwavelength Selected Areas." Figure 10.11 demonstrates that AGN SEDs are well probed across a broad range of wavelengths both in terms of depth and areal coverage. LSST AGN with multiwavelength data available will have less selection bias than AGN selected by LSST optical colors alone (§ 10.1), allowing large samples to be constructed that are representative of the overall AGN population. Combining multi-wavelength data sets with the LSST optical catalogs will also reveal new views of the wide range of AGN phenomena.

For example, overlapping X-ray observations will be a valuable component of source-classification algorithms for LSST AGN; X-ray-to-optical flux ratios of AGN are roughly $\sim 0.1 - 10$ (e.g., Schmidt et al. 1998; Barger et al. 2003; Bauer et al. 2004). The ROSAT All-Sky Survey (Voges et al. 1999) and the XMM-Newton Slew Survey (Saxton et al. 2008) will overlap the LSST survey region, giving at least shallow to moderate-depth X-ray coverage to nearly all LSST AGN. There are already $\sim 10^2$ deg^2 of sky covered with Chandra to a depth sufficient to detect 10^2 AGN deg^{-2} (e.g., Green et al. 2009), and of course this area will continue to expand. LSST imaging of the Chandra Deep Field South region in the "deep drilling" LSST mode (§ 2.1) will enable detailed studies of heavily obscured AGN. Although such deep Chandra data are concentrated in a few pencil-beam fields, they yield very impressive AGN surface densities of ~ 7000 deg^{-2}, and the obscured sources

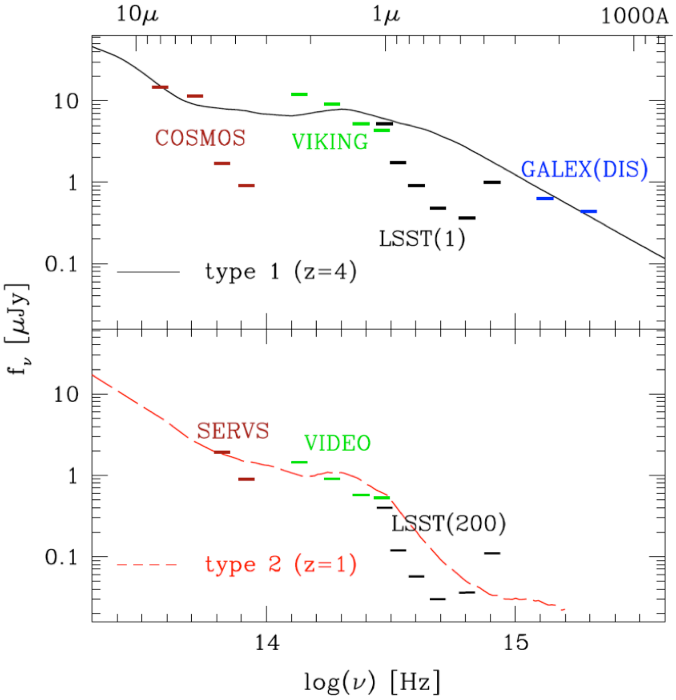

Figure 10.11: *top:* Type 1 quasar SED (Richards et al. 2006a) at $z = 4$ compared to the overlapping depth of the COSMOS (Sanders et al. 2007) data in the mid-IR, the proposed VISTA-VIKING (Arnaboldi et al. 2007) survey in the near-IR, the LSST single epoch data in the optical, and the GALEX (Martin et al. 2005) Deep Imaging Survey (DIS) in the UV. *bottom:* Type 2 quasar SED (Zakamska et al. 2003) at $z = 1$ compared to the overlapping depth of the SERVS (Lacy & SERVS team 2009), VISTA-VIDEO (Arnaboldi et al. 2007), and multi-epoch LSST surveys.

comprise a significant fraction of the AGN population that are missed by shallower optical surveys (e.g., Brandt & Hasinger 2005). X-ray observations can also reveal important AGN characteristics that can be compared to optically-derived measures of spectral shape, luminosity, and temporal evolution. For example, the X-ray SED slope (represented by the ratio between hard and soft X-ray flux) is an indicator of X-ray absorption, and can be used to classify Type 2 AGN (e.g., Mainieri et al. 2002).

Heavily obscured LSST AGN may also be identified by combining LSST optical colors with sub-millimeter surveys (e.g., Alexander et al. 2005), or mid-IR photometry from Spitzer (e.g., Polletta et al. 2006). There are of order $10^2\,\mathrm{deg}^2$ of deep mid-IR imaging data from surveys like SWIRE (Lonsdale et al. 2003); these surveys have AGN surface densities approaching $10^3\,\mathrm{deg}^{-2}$. Combining LSST data with these surveys and X-ray data may even be used to identify Compton thick AGNs, and mid-infrared photometry can also improve photometric redshift estimates over purely optical estimates. Cross-correlating mid–far-IR data (e.g., from Spitzer and Herschel) with LSST AGN will also improve our understanding of the starburst-AGN connection across cosmic time.

Radio survey data of LSST AGN will allow us to distinguish between radio-loud and radio-quiet AGN, test the dependence of radio power on luminosity and redshift, and probe unification models. The combination of X-ray, radio, and LSST photometry may identify new blazars from their unusual location in X-ray-radio-optical multi-band diagrams (e.g., Perlman et al. 2001). Additional gamma-ray information from the Fermi Gamma-ray Space Telescope will improve our understanding of how accretion processes accelerate immense jets of material to nearly the speed of light. Although only early Fermi results are available at the time of writing, more than $\sim 10^3$ gamma-ray blazars may be selected and monitored at high energies (e.g., Abdo et al. 2009). Moreover, LSST may contribute significantly to Fermi blazar identifications: for example, LSST may discover transient/variable optical objects coincident with radio sources and inside Fermi persistent gamma-ray error circles, or transients/variables may be caught flaring contemporaneously in both LSST and Fermi. Blazars display dramatic SED changes, which are associated with the jet acceleration mechanism. LSST will provide optical light curve information on few day (or better) timescales for 10^{2-3} Fermi blazars (with $m > 17$) in the LSST sky region; Fermi's lifetime will plausibly suffice to provide extraordinary contemporaneous blazar gamma-ray lightcurves extending down to intra-day time resolution, for high-energy comparison to corresponding LSST optical lightcurves of the full ensemble.

Multiwavelength data for the LSST AGN census will produce the largest inventory of AGN SEDs over a very wide wavelength range, allowing better constraints on typical accretion and reprocessing mechanisms. A combination of multiwavelength data from optical, radio, infrared, ultraviolet, and X-ray bands is also essential to avoid missing "drop-outs" from sources that are atypically faint in some wavebands, including such interesting classes as high-redshift AGN, obscured AGN (e.g., Brandt & Hasinger 2005), "X-ray bright, optically-normal galaxies" (XBONGs; e.g., Comastri et al. 2002), or intrinsically X-ray weak AGN (e.g., Just et al. 2007; Leighly et al. 2007). LSST will likely also discover interesting AGN that cannot be straightforwardly classified based on their multiwavelength properties, highlighting the most promising subset for follow-up. Such sources may include remarkable outliers, "borderline" sources in classification schemes, as well as interesting classes of AGN that are strongly distinguished by their unusual radio, infrared, optical-UV, and/or X-ray colors.

10.4.2 Time-Dependent SEDs

Augmenting LSST photometry with multiwavelength data will also enable unprecedented temporal investigations. For example, AGN that flare or exhibit other unusual temporal behavior in LSST will trigger alerts for multiwavelength follow-up in other relevant energy bands. In principle, these alert criteria could be quite complex, identifying the onset of strong absorption or a "state change" in the variation properties (§ 10.5). In such cases, it will be particularly interesting to obtain multiwavelength observations to determine how the inner AGN regions (e.g., the jet base or disk corona) are affected.

LSST will, over its lifetime, measure optical variation amplitudes and colors for AGN over a wide range of luminosities and redshifts. Hundreds of repeat LSST observations in each band will reveal the extent to which the scatter in measured SED shapes (e.g., Steffen et al. 2006; Gibson et al. 2008a) can be attributed to emission or absorption variability over observed time scales of days to a few years. Additionally, any AGN in the LSST sky coverage targeted contemporaneously (purposefully or serendipitously) in another energy band by future ground- or space-based observations can be matched to the most recent LSST optical photometry in order to derive statistical inferences about the shape of the AGN SED and its evolution on shorter time scales.

SED variation will be particularly interesting for strongly-absorbed AGN in order to constrain the size scales, evolution, lifetimes, and large-scale impact of absorbing outflows. As one example, Broad absorption line (BAL) outflows, and their AGN hosts, have been studied in the radio, infrared, optical-UV, and X-rays (e.g., Gibson et al. 2009, and references therein). Their SEDs reveal information about the structure and evolution of UV and X-ray absorbers in the central region of an AGN. LSST will monitor the light curves and colors of the $\sim$ 5000 BAL quasars identified in current catalogs (Gibson et al. 2009), and (at least) thousands more will be identified in the LSST fields by SDSS–III and future surveys. LSST monitoring will enable other observatories to trigger follow-up observations based on dramatic changes in the absorption of these sources, and will provide detailed light curves useful for studies of absorber photoionization. Multi-wavelength follow-up observations will examine connections among the various structures that absorb radiation in the different wavebands.

In some cases, AGN have demonstrated coordinated variability across multiple wavebands that is presumably driven by physical relations among the structures responsible for emission in each waveband (e.g., Uttley & Mchardy 2004). Coordinated campaigns to monitor AGN in other wavebands could, in principle, generate multi-wavelength light curves for large numbers of AGN (or for interesting classes of AGN) sampled on rest-frame time scales of days or shorter. Because SED wavebands are associated with different physical processes, the correlations (including lead or lag times) between wavebands can reveal relationships among emitting structures such as the accretion disk and its corona.

10.5 AGN Variability

W. N. Brandt, Willem H. de Vries, Paulina Lira, Howard A. Smith

One of the key characteristics of AGNs is that their emission is variable over time. In addition to aiding effective AGN selection (see § 10.1), this time dependence offers a probe of the physics associated with the accretion process. While there is no model capable of explaining all aspects of AGN variability in a compelling manner, accretion-disk instabilities, changes in accretion rate, the evolution of relativistic jets, and line-of-sight absorption changes have all been invoked to model the observed variability.

The characteristics of AGN variability are frequently used to constrain the origin of AGN emission (e.g., Kawaguchi et al. 1998; Trèvese et al. 2001; Kelly et al. 2009). AGN variability is observed to depend upon luminosity, wavelength, time scale, and the presence of strong radio jets. However, despite considerable efforts over last few decades, conflicting claims about correlations with physical properties exist. This is at least in part due to the fact that many early studies included at most only 50–300 objects and had a limited number of observation epochs (see Giveon et al. 1999; Helfand et al. 2001).

Significant progress in the description of AGN variability has recently been made by employing SDSS data (de Vries et al. 2003, 2005; Vanden Berk et al. 2004; Ivezić et al. 2004; Wilhite et al. 2005, 2006; Sesar et al. 2006). Vanden Berk et al. (2004) used two-epoch photometry for 25,000 spectroscopically confirmed quasars to constrain how quasar variability in the optical/UV regime depends upon rest-frame time scale (up to $\sim$ 2 years in the observed frame), luminosity, rest wavelength, redshift, and other properties. They found that accretion-disk instabilities are the most likely mechanism causing the majority of observed variability. de Vries et al. (2005) and Sesar et al. (2006) utilized SDSS and Palomar Observatory Sky Survey (POSS) measurements for 40,000 quasars spectroscopically confirmed by SDSS, and constrained quasar continuum variability on time scales of 10–50 yr in the observer's frame. In the context of a shot-noise light-curve model, de Vries et al. (2005) found evidence for multiple variability timescales in long-term variability measurements. Using SDSS repeat spectroscopic observations obtained more than 50 days apart for 315 quasars which showed significant variations, Wilhite et al. (2005) demonstrated that the difference spectra are bluer than the ensemble quasar spectrum for rest-frame wavelengths shorter than 2500 Å with very little emission-line variability. The difference spectra in the rest-frame wavelength range 1300–6000 Å could be fit by a standard thermal accretion-disk model with a variable accretion rate (Pereyra et al. 2006).

However, the above efforts were limited in what they could study, given that each object in their sample was observed only twice. The LSST variability survey will be unrivaled in its combination of size (millions of AGNs), number of observation epochs, range of timescales probed (rest-frame minutes-to-years), multi-color coverage, and photometric accuracy. Relations between AGN variability properties and luminosity, redshift, rest-frame wavelength, time scale, color, radio-jet emission, and other properties will be defined with overwhelming statistics over a wide range of parameter space. Degeneracies between the potential controlling parameters of variability will thereby be broken, enabling reliable determination of which parameters are truly fundamental. With appropriate spectroscopic follow-up, it will also be possible to relate AGN variability to emission-line and absorption-line properties, as well as physical parameters including black-hole mass and Eddington-normalized luminosity (e.g., O'Neill et al. 2005). Both the observed luminosity and spectral variability of the optical/UV AGN continuum will used to test accretion and jet models.

The LSST AGN variability survey will also greatly improve our categorization of the range and kinds of AGN variability. Rare but physically revealing events, for example, will be detected in sufficient numbers for useful modeling. These are expected to include transient optical/UV obscuration events due to gas and dust moving temporarily into the line of sight (e.g., Goodrich 1995; Lundgren et al. 2007; Gibson et al. 2008b), strong intranight variability events (e.g., Stalin et al. 2005; Czerny et al. 2008), and perhaps quasi-periodic oscillations. Notable events discovered by LSST will trigger rapid follow-up with other facilities, and LSST photometry will automatically synergize with many AGN monitoring efforts (e.g., wide-field X-ray and gamma-ray monitors; reverberation-mapping projects). AGN lifetimes, or at least the timescales over which they make accretion-state transitions, will also be constrained directly by looking for objects that either rise or drop strongly in flux (e.g., Martini & Schneider 2003).

10.6 Transient Fueling Events: Temporary AGNs and Cataclysmic AGN Outbursts

Aaron J. Barth, W. N. Brandt, Michael Eracleous, Mark Lacy

Strong transient outbursts from galactic nuclei can occur when a star, planet, or gas cloud is tidally disrupted and partially accreted by a central SMBH. The tidal field of a SMBH is sufficient to disrupt solar-type stars that approach within $\sim 5M_7^{-2/3}$ Schwarzschild radii, where $M_{SMBH} = M_7 \times 10^7 M_\odot$ (Hills 1975). An optical flare lasting several months is expected when the star disintegrates outside the event horizon, i.e., for $M_7 < 20$. Transient variability may also arise during the inspiral and merger phases of binary SMBHs. LSST will be a premier facility for discovering and monitoring such transient SMBH phenomena, enabling and aiding studies across the electromagnetic spectrum as well as detections with gravitational waves.

10.6.1 Tidal Disruption Events by Supermassive Black Holes

Models of tidal disruptions predict optical emission from a hot optically thick accretion disk dominating the continuum and enhanced by line emission from unbound ejecta (Roos 1992; Ulmer 1999). The peak brightness can reach $M_R = -14$ to -19 mag approaching that of a supernova. The expected full sky rate of events down to a 24 mag threshold (z $\sim$ 0.3) is $10^4 M_7^{3/2}$ yr^{-1}. Multi-epoch X-ray and UV observations have discovered about eight candidates for tidal-disruption events in the form of large-amplitude nuclear outbursts (e.g., Donley et al. 2002; Komossa et al. 2004; Vaughan et al. 2004; Gezari et al. 2006, 2008). These events have large peak luminosities of $\sim 10^{43}$–10^{45} erg s^{-1}, optical-to-X-ray spectral properties broadly consistent with those expected from tidal disruptions, and decay timescales of months. The inferred event rate per galaxy is 10^{-5}–10^{-4} yr^{-1} (Donley et al. 2002; Gezari et al. 2008; Luo et al. 2008), roughly consistent with the predicted rate for stellar tidal disruptions (e.g., Wang & Merritt 2004). These X-ray and UV outbursts are theoretically expected and in some cases observed (Brandt et al. 1995; Grupe et al. 1995; Gezari et al. 2008) to induce accompanying optical nuclear variability that will be detectable by LSST.

LSST will dramatically enlarge the sample of detected tidal-disruption events, thereby providing by far the best determination of their rate. Gezari et al. (2008) and Gezari et al. (2009) have used the currently known UV/optical events to estimate rates, and predict that LSST should detect at least 130 tidal disruptions per year. With such a large sample, it will be possible to measure outburst rates as a function of redshift, host-galaxy type, and level of nuclear activity. This will allow assessment of the role that tidal disruptions play in setting the luminosity function of moderate-luminosity active galaxies (e.g. Milosavljević et al. 2006).

An interesting subset of tidal-disruption events involves the disruption of a white dwarf by a black hole of mass $< 10^5$ M$_\odot$ (e.g., Rosswog et al. 2008; Sesana et al. 2008). Such events are interesting for the following reasons. First, the debris released from the disruption of a white dwarf is virtually devoid of hydrogen, giving rise to a unique spectroscopic signature. Second, since white dwarfs are tightly bound objects, their tidal disruption radius is smaller than the Schwarzschild radius of a black hole for black hole masses greater than 2×10^5 M$_\odot$. In other words, black holes more massive than this limit will swallow white dwarfs whole without disrupting them. Third, unlike main sequence stars, the strong tidal compression during the disruption of a white dwarf triggers thermonuclear reactions which release more energy than the gravitational binding energy of the white dwarf (Rosswog et al. 2008). Thus, such an event could resemble a supernova, albeit with a different light curve and a different spectral evolution. Fourth, the disruption of a white dwarf in an initially bound orbit around a black hole is accompanied by a strong gravitational wave signal, detectable by LISA, considerably stronger than that of a main sequence star.

Detection of the prompt optical flash of such a white dwarf disruption event with the LSST would allow rapid follow-up spectroscopy to confirm the nature of the event through the composition of the debris and the shape of the light curve. Such events are of particular interest because they can reveal the presence of moderately massive black holes in the nuclei of (presumably dwarf) galaxies. Black holes in this mass range are "pristine" examples of the seeds that grow to form the most massive black holes known today (see Volonteri 2008, and references therein). As such they provide useful constraints on models of hierarchical galaxy assembly and growth of their central black holes.

The tidal disruption events that have been discovered to date were mostly identified after they were largely over. However, LSST data processing will provide near-instant identification of transient events in general and new tidal disruptions in particular (§ 2.5), so that intensive optical spectroscopic and multiwavelength follow-up studies will be possible while the events are in their early stages. Prompt and time-resolved optical spectroscopy, for example, will allow the gas motions from the tidally disrupted object to be traced and compared with computational simulations of such events (e.g., Bogdanović et al. 2004). Joint observations with LSST and X-ray missions such as the Black Hole Finder Probe (e.g., Grindlay 2005), JANUS, and eROSITA will allow the accreting gas to to be studied over the broadest possible range of temperatures and will also constrain nonthermal processes such as Compton upscattering and shocks. LSST identifications of tidal disruptions will also complement LISA detections as these events are expected to create gravitational-wave outbursts (e.g., Kobayashi et al. 2004).

10.6.2 Inspirals of Binary Supermassive Black Holes

SMBH mergers are an expected component of models of galaxy evolution and SMBH growth. The correlation of the masses of the central SMBHs in galaxies today and the velocity dispersions of their bulges suggests a close link between the build-up of mass in galaxies and in their central SMBHs, perhaps driven by mergers, as many models suggest (e.g., Kauffmann & Haehnelt 2000; Di Matteo et al. 2008).

Several dual SMBH systems have already been found in the form of quasar pairs, but most have relatively wide ($\sim$ 10 kpc) separations (Hennawi et al. 2006, Comerford et al. 2008). At lower redshift, there are now several examples of dual AGN with $\sim$ kpc separation in merging galaxies, the best-known case being NGC 6240 (e.g., Komossa et al. 2003). True binary systems, in which the two SMBHs are tightly gravitationally bound to each other, have proved more difficult to find, and the single nearby example is a binary with 7 pc separation discovered in the radio with VLBI (Rodriguez et al. 2006). Theory indicates that dynamical friction will cause the SMBHs in galaxy merger events to sink to the bottom of the common potential well formed at the end of the merger on a timescale of $\sim 10^7$ yr. There they form a SMBH binary system with pc-scale separation, primarily by ejecting stars from the core of the galaxy (e.g., Begelman et al. 1980). These binary systems may be, however, resistant to further decay (Yu 2002) until the separation reaches less than about 10^{-3} pc, when gravitational radiation becomes an effective mechanism for angular momentum loss (the "inspiral" phase).

The solution to the stalling of the binary separation at the parsec scale probably lies in gas. In the most-likely case of an unequal mass merger, an accretion disk around the primary SMBH can exert a torque on the secondary component, reducing its angular momentum over a period of $\sim 10^7$ yr (e.g., Armitage & Natarajan 2002). Furthermore, in this scenario, a spike in the accretion rate will occur during the inspiral phase as gas trapped between the two SMBHs is accreted (over a period of $\sim 10^3$ yr). More detailed predictions of the accretion rate as a function of time during the binary phase were performed by Cuadra et al. (2009). They argue that the accretion rate onto both SMBHs will vary on timescales corresponding to the binary period. For example, a ~ 0.01 pc separation of two $\sim 3 \times 10^6\ M_\odot$ SMBHs leads to a variability period of ~ 1 month, well suited for detection within the enormous sample of LSST AGN with high-quality photometric monitoring.

Another prominent observational signature of sub-pc binaries can come about from the interaction of one of the two black holes with the accretion disk surrounding the other. Such an interaction (and the resulting signal) is likely to be periodic, but with periods on the order of decades to centuries. Thus, we are likely to observe individual events and perceive them to be isolated flares. Some initial theoretical work attempting to predict the observational signature of such an interaction has been carried out by Bogdanović et al. (2008). Candidates for such systems have also been found. The best known example is OJ 287 where more than a dozen pairs of outbursts have been observed with a recurrence time between pairs of 10–12 years (e.g., Valtonen 2007; Valtonen et al. 2008, and references therein). Less persuasive claims for recurring outbursts have also been made for 3C 390.3 and PKS 0735+178 (Qian & Tao 2004; Tao et al. 2008). The role of the LSST in identifying similar outbursts will be extremely important. After the initial identification, candidates can be studied further with continued long-term photometry and spectroscopy, in order to verify the nature of the system and derive its properties.

10.6.3 Mergers of Binary Supermassive Black Holes

The proposed gravitational wave telescope LISA will have the capability to detect gravitational waves from SMBH mergers out to $z \sim 10$ or higher. In favorable cases, LISA will be able to localize a source to within a few arc-minutes to a few degrees on the sky. Furthermore, the gravitational-wave signal from binary SMBH coalescence serves as a "standard siren" that gives the luminosity distance to the event (limited by uncertainties in gravitational lensing along the line-of-sight), so LISA can provide a three-dimensional localization for a detected event. Determination of the luminosity distance is possible because the shape of the gravitational waveform (i.e., the variation of the frequency as a function of time) depends on the *chirp* mass of the binary ($\mathcal{M} \equiv [(M_1 M_2)^3/(M_1 + M_2)]^{1/5}$, where M_1 and M_2 are the masses of the two components), while the amplitude of the wave depends on the ratio of the chirp mass to the luminosity distance (Hughes 2009). Therefore, fitting the waveform yields the chirp mass, which can then be combined with the measured amplitude to yield the luminosity distance. The uncertainty in the luminosity distance is ultimately set by the signal-to-noise ratio of the gravitational-wave amplitude (see Finn & Chernoff 1993). Identification of the electromagnetic counterparts to such events will be of great importance, both for studying the physics of accretion during SMBH mergers (e.g., Milosavljević & Phinney 2005) and for measurement of the redshift. The redshift can be combined with the luminosity distance measured by LISA to provide new constraints on cosmological parameters (e.g. Holz & Hughes 2005).

The LSST data stream has the potential to be one of the most important resources for identifying the electromagnetic counterparts to SMBH mergers. During the final month before SMBH coalescence, there may be a periodic signature in the accretion luminosity due to the binary orbit, with a period of minutes to hours. The electromagnetic afterglow following the coalescence may be primarily luminous in X-rays (Milosavljević & Phinney 2005), but reprocessing or ionization of emission-line gas could make the source detectable in the optical and near-infrared. And once the coalescence takes place, LSST will be able to localize the host object (Kocsis et al. 2006). Indeed, the LISA error volume in angle and distance may be small enough to identify the object uniquely, given LSST's photometric redshifts and AGN identification.

10.7 Gravitationally Lensed AGNs

W. N. Brandt, George Chartas

As discussed in the strong lens chapter (§ 12.2), we estimate that in its single-visit images, LSST will discover ~ 4000 luminous AGN that are gravitationally lensed into multiple images (§ 12.8). This more than ten-fold increase in the number of known gravitationally-lensed quasar systems, combined with the high cadence of observations of these systems will allow a variety of studies of these systems. We discuss the lensing-specific issues in § 12.8, while here we focus on what we can learn about the AGN themselves.

10.7.1 Microlensing as a Probe of AGN Emission Regions

Resolving the emission regions of distant quasars is beyond the capabilities of present-day telescopes, and thus indirect methods have been applied to explore these regions. Such methods include reverberation mapping of the broad line region (e.g., Peterson 1993; Netzer & Peterson 1997), measurements of occultations of the central X-ray source by absorbing clouds (Risaliti et al. 2007), and microlensing of the continuum and emission-line regions (e.g., Grieger et al. 1988, 1991; Schneider et al. 1992; Gould & Gaudi 1997; Agol & Krolik 1999; Mineshige & Yonehara 1999; Yonehara et al. 1999; Chartas et al. 2002; Popović et al. 2003; Blandford et al. 2006; Kochanek et al. 2007; Pooley et al. 2006, 2007; Jovanović et al. 2008; Morgan et al. 2008).

Since LSST will be monitoring the fluxes of $\simeq 4000$ gravitationally lensed AGN, it is ideally suited to tracking microlensing events in these systems. These events are produced by the lensing effect of a star or group of stars in the lensing galaxy. As the caustic network produced by the stars traverses the AGN accretion disk and other emission sources, regions near the caustics will be magnified. This causes uncorrelated variability in the brightnesses of the images of a lensed quasar, where the amplitude of the variability is determined by the ratio of the emission regions to the Einstein radius (e.g., Lewis et al. 1998; Popović & Chartas 2005). The largest components, such as the radio and optical emission-line regions, should show little or no microlensing variability. The thermal continuum emission from the disk should show greater variability at shorter wavelengths, corresponding to smaller disk radii and higher temperatures. This wavelength dependent variability has been observed by Anguita et al. (2008) and Poindexter et al. (2008), and LSST should enable its study for large numbers of gravitationally lensed AGN.

The timescale of a microlensing event will depend in general on the size of the source, the relative transverse velocity of the caustic with respect to the source, and the angular diameter distances $D_{\rm os}$ and $D_{\rm ol}$, where the subscripts o, s, and l refer to the observer, source, and lens respectively. The caustic crossing time can be expressed as $t_{\rm cross} = (1 + z_{\rm lens})(R_{\rm source}/v)(D_{\rm ol}/D_{\rm os})$, where $z_{\rm lens}$ is the redshift of the lens, $R_{\rm source}$ is the size of the emitting region, and v is the relative transverse velocity of the caustic with respect to the source. Thus, for AGNs with redshifts in the range of 1–4 we expect typical timescales for a caustic to cross the optical emission region of the disk to be of the order of a few weeks. The cadence of LSST is, therefore, well suited to map out microlensing light curves of AGNs.

10.7.2 LSST Microlensing Constraints on Accretion Disks

The first step in large scale LSST microlensing studies will necessarily be the identification of the lensed AGN. Good candidates for lensed AGN will be identified using photometric redshift information for objects with small angular separations. These candidates may then be confirmed either via follow-up spectroscopic observations or via LSST studies of intrinsic variability. In the latter case, one will be searching for similar light curves from the putative lensed AGN images that are temporally shifted due to the different light-travel times associated with each image. The detection in deep LSST images of a foreground galaxy or cluster that could act as the lens will also aid the identification process and allow lenses to be distinguished from binary quasars.

Once the light-travel time delay is determined via a cross-correlation analysis from a given lens light curve, the data can be searched for evidence of microlensing. The LSST cadence will be sufficient for many microlensing analyses. However, to obtain even better temporal sampling (e.g., for rare, high-magnification events that have relatively short duration), it will make sense to target identified microlensing events with additional telescopes. Ultraviolet and X-ray observations using facilities with sufficient angular resolution, such as Chandra in the X-ray band, will also be pursued as appropriate.

The large number of lensed quasars from $z \approx 1$–6 will allow a search for evolution of AGN structure across this redshift range and a large range of luminosity and Eddington ratio. For example, a change in the mode of accretion from the standard thin accretion-disk solution may be revealed by changes in the scalings between wavelength, emission radius, and SMBH mass. Microlensing analyses will help to determine whether the observed "downsizing" in the luminosity function (§ 10.2) is accompanied by downsizing in accretion-disk size and SMBH mass.

10.8 Public Involvement with Active Galaxies and Supermassive Black Holes

W. N. Brandt, Ohad Shemmer

Active galaxies and the supermassive black holes that power them are of strong interest to the public. LSST will greatly advance understanding of both the demography and physics of active galaxies, and thus there are numerous approaches that can be used to involve non-astronomers in LSST active-galaxy discoveries. Effective themes for engaging the public include understanding the engines of the most powerful sources in the Universe, using active galaxies to trace large-scale structures, and finding the most distant cosmic objects.

Advanced high-school students, college students, and science teachers (at the elementary school through high school levels) can learn about the methods by which LSST finds active galaxies by working with multi-color and multi-epoch LSST images. These students will categorize the various types of cosmic objects LSST detects using their color and variability properties, and then isolate the ranges of these properties corresponding to active galactic nuclei (for example, strong blue emission and significant variability). This can lead to discussions of why active galaxies have the colors they do (i.e., accretion disks around supermassive black holes), the sizes and structures of their central engines, and extreme strong-gravity conditions. Special rare cases of color and variability behaviors will be used to explore remarkable objects. For example, the highest redshift quasars found by LSST that probe the cosmic dark ages will appear in only the reddest filter. Similarly, remarkable variability can be used to identify transient fueling events of supermassive black holes by stellar tidal disruptions.

We will include computer-based modules on the LSST World Wide Web site that will illustrate basic LSST active galaxy concepts to the general public. These will include a tool that shows the connection between an active galaxy's spectrum and its multi-band LSST images (with connections to photometric redshifts for advanced learners) and interactive three-dimensional movies of the Universe as traced by the LSST AGN population. These modules will also include elementary school activities such as building, with basic materials (e.g., beads and string), a patch of the Universe based on LSST active-galaxy large-scale structure data.

Dedicated amateur astronomers acting as "Citizen Scientists," including faculty and students at small colleges and high schools, can play a valuable role by spectroscopically investigating remarkable bright LSST active galaxy phenomena. For example, amateur groups with access to telescopes of 32″ or more using modern spectrographs can study the optical spectra of many $m_{\rm r} < 19$ AGN that LSST will detect during its 10-year mission. Such studies may also include real-time spectroscopy of active-galaxy flares and spectroscopic variability monitoring aimed at revealing active-galaxy structure. This will allow the Citizen Scientists to complement the research of professional astronomers by making many instruments available at a particular moment of interest with the advantage of increased flexibility and shortening of observational response times. Citizen Scientists will also be employed to classify the morphologies of nearby active galaxies via an "Active Galaxy Zoo" (see § 4.5 and § 9.11).

References

Abdo, A. A. et al., 2009, *ApJ*, 700, 597

Agol, E., & Krolik, J., 1999, *ApJ*, 524, 49

Alexander, D. M., Bauer, F. E., Chapman, S. C., Smail, I., Blain, A. W., Brandt, W. N., & Ivison, R. J., 2005, *ApJ*, 632, 736

Anguita, T., Schmidt, R. W., Turner, E. L., Wambsganss, J., Webster, R. L., Loomis, K. A., Long, D., & McMillan, R., 2008, *A&A*, 480, 327

Armitage, P. J., & Natarajan, P., 2002, *ApJL*, 567, L9

Arnaboldi, M., Neeser, M. J., Parker, L. C., Rosati, P., Lombardi, M., Dietrich, J. P., & Hummel, W., 2007, *The Messenger*, 127, 28

Barger, A. J., Cowie, L. L., Capak, P., Alexander, D. M., Bauer, F. E., Brandt, W. N., Garmire, G. P., & Hornschemeier, A. E., 2003, *ApJL*, 584, L61
Bauer, F. E., Alexander, D. M., Brandt, W. N., Schneider, D. P., Treister, E., Hornschemeier, A. E., & Garmire, G. P., 2004, *AJ*, 128, 2048
Beck-Winchatz, B., & Anderson, S. F., 2007, *MNRAS*, 374, 1506
Beers, T. C., & Sommer-Larsen, J., 1995, *ApJS*, 96, 175
Begelman, M. C., Blandford, R. D., & Rees, M. J., 1980, *Nature*, 287, 307
Bernstein, G. M., 1994, *ApJ*, 424, 569
Blandford, R. D., Oguri, M., Marshall, P., Baltz, E. A., Bradac, M., Fassnacht, C. D., & LSST collaboration, 2006, American Astronomical Society Meeting Abstracts, 209, 86.12
Bock, D. C.-J., Large, M. I., & Sadler, E. M., 1999, *AJ*, 117, 1578
Bogdanović, T., Eracleous, M., Mahadevan, S., Sigurdsson, S., & Laguna, P., 2004, *ApJ*, 610, 707
Bogdanović, T., Smith, B. D., Sigurdsson, S., & Eracleous, M., 2008, *ApJS*, 174, 455
Braccesi, A., Formiggini, L., & Gandolfi, E., 1970, *A&A*, 5, 264
Brandt, W. N., & Hasinger, G., 2005, *ARAA*, 43, 827
Brandt, W. N., Pounds, K. A., & Fink, H., 1995, *MNRAS*, 273, L47
Burrows, D. N., 2009, in Bulletin of the American Astronomical Society, Vol. 41, Bulletin of the American Astronomical Society, p. 487
Chartas, G., Agol, E., Eracleous, M., Garmire, G., Bautz, M. W., & Morgan, N. D., 2002, *ApJ*, 568, 509
Coil, A. L., Hennawi, J. F., Newman, J. A., Cooper, M. C., & Davis, M., 2007, *ApJ*, 654, 115
Comastri, A. et al., 2002, *ApJ*, 571, 771
Comerford, J. M. et al., 2008, ArXiv e-prints, 0810.3235
Condon, J. J., Cotton, W. D., Greisen, E. W., Yin, Q. F., Perley, R. A., Taylor, G. B., & Broderick, J. J., 1998, *AJ*, 115, 1693
Cowie, L. L., Songaila, A., Hu, E. M., & Cohen, J. G., 1996, *AJ*, 112, 839
Croom, S. M. et al., 2009a, *MNRAS*, 392, 19
—, 2009b, ArXiv e-prints, 0907.2727
Croom, S. M., Smith, R. J., Boyle, B. J., Shanks, T., Miller, L., Outram, P. J., & Loaring, N. S., 2004, *MNRAS*, 349, 1397
Cuadra, J., Armitage, P. J., Alexander, R. D., & Begelman, M. C., 2009, *MNRAS*, 393, 1423
Czerny, B., Siemiginowska, A., Janiuk, A., & Gupta, A. C., 2008, *MNRAS*, 386, 1557
de Vries, W. H., Becker, R. H., & White, R. L., 2003, *AJ*, 126, 1217
de Vries, W. H., Becker, R. H., White, R. L., & Loomis, C., 2005, *AJ*, 129, 615
Di Matteo, T., Colberg, J., Springel, V., Hernquist, L., & Sijacki, D., 2008, *ApJ*, 676, 33
Djorgovski, S., 1991, Astronomical Society of the Pacific Conference Series, 21, 349
Donley, J. L., Brandt, W. N., Eracleous, M., & Boller, T., 2002, *AJ*, 124, 1308
Eisenhardt, P. R. et al., 2009, Bulletin of the American Astronomical Society, Vol. 41, WISE: The Wide-field Infrared Survey Explorer. p. 363
Eisenstein, D. J. et al., 2005, *ApJ*, 633, 560
Fan, X., 1999, *AJ*, 117, 2528
Fan, X. et al., 2006a, *AJ*, 132, 117
—, 2006b, *AJ*, 131, 1203
—, 2001, *AJ*, 121, 54
Ferrarese, L., 2002, *ApJ*, 578, 90
Finn, L. S., & Chernoff, D. F., 1993, *Phys. Rev. D*, 47, 2198
Gezari, S. et al., 2008, *ApJ*, 676, 944
—, 2006, *ApJL*, 653, L25
—, 2009, *Astronomy*, 2010, 88
Gibson, R. R., Brandt, W. N., & Schneider, D. P., 2008a, *ApJ*, 685, 773
Gibson, R. R., Brandt, W. N., Schneider, D. P., & Gallagher, S. C., 2008b, *ApJ*, 675, 985
Gibson, R. R. et al., 2009, *ApJ*, 692, 758
Giveon, U., Maoz, D., Kaspi, S., Netzer, H., & Smith, P. S., 1999, *MNRAS*, 306, 637
Goodrich, R. W., 1995, *ApJ*, 440, 141
Gould, A., & Gaudi, B. S., 1997, *ApJ*, 486, 687
Green, P. J. et al., 2009, *ApJ*, 690, 644
Grieger, B., Kayser, R., & Refsdal, S., 1988, *A&A*, 194, 54

Grieger, B., Kayser, R., & Schramm, T., 1991, *A&A*, 252, 508
Grindlay, J. E., 2005, *New Astronomy Review*, 49, 436
—, 2009, Bulletin of the American Astronomical Society, Vol. 41, The Energetic X-ray Imaging Survey Telescope (EXIST). p. 388
Grupe, D., Beuermann, K., Mannheim, K., Bade, N., Thomas, H.-C., de Martino, D., & Schwope, A., 1995, *A&A*, 299, L5
Hartwick, F. D. A., & Schade, D., 1990, *ARAA*, 28, 437
Hasinger, G., Miyaji, T., & Schmidt, M., 2005, *A&A*, 441, 417
Helfand, D. J., Stone, R. P. S., Willman, B., White, R. L., Becker, R. H., Price, T., Gregg, M. D., & McMahon, R. G., 2001, *AJ*, 121, 1872
Hennawi, J. F., & Prochaska, J. X., 2007, *ApJ*, 655, 735
Hennawi, J. F. et al., 2006, *AJ*, 131, 1
Hewett, P. C., Foltz, C. B., & Chaffee, F. H., 1993, *ApJL*, 406, L43
Hills, J. G., 1975, *Nature*, 254, 295
Holberg, J. B., & Bergeron, P., 2006, *AJ*, 132, 1221
Holz, D. E., & Hughes, S. A., 2005, *ApJ*, 629, 15
Hopkins, P. F., Hernquist, L., Cox, T. J., Di Matteo, T., Robertson, B., & Springel, V., 2006, *ApJS*, 163, 1
Hopkins, P. F., Lidz, A., Hernquist, L., Coil, A. L., Myers, A. D., Cox, T. J., & Spergel, D. N., 2007a, *ApJ*, 662, 110
Hopkins, P. F., Richards, G. T., & Hernquist, L., 2007b, *ApJ*, 654, 731
Hughes, S. A., 2009, ArXiv e-prints, 0903.4877
Ivezić, Ž. et al., 2003, *Memorie della Societa Astronomica Italiana*, 74, 978
Ivezić, Ž.. et al., 2004, in IAU Symposium, Vol. 222, The Interplay Among Black Holes, Stars and ISM in Galactic Nuclei, T. Storchi-Bergmann, L. C. Ho, & H. R. Schmitt, eds., pp. 525–526
Jansen, F. et al., 2001, *A&A*, 365, L1
Jiang, L. et al., 2008, *AJ*, 135, 1057
—, 2009, *AJ*, 138, 305
—, 2006, *AJ*, 131, 2788
Jovanović, P., Zakharov, A. F., Popović, L. Č., & Petrović, T., 2008, *MNRAS*, 386, 397
Just, D. W., Brandt, W. N., Shemmer, O., Steffen, A. T., Schneider, D. P., Chartas, G., & Garmire, G. P., 2007, *ApJ*, 665, 1004
Kaczmarczik, M. C., Richards, G. T., Mehta, S. S., & Schlegel, D. J., 2009, *AJ*, 138, 19
Kauffmann, G., & Haehnelt, M., 2000, *MNRAS*, 311, 576
Kawaguchi, T., Mineshige, S., Umemura, M., & Turner, E. L., 1998, *ApJ*, 504, 671
Kelly, B. C., Bechtold, J., & Siemiginowska, A., 2009, ArXiv e-prints, 0903.5315
Kobayashi, S., Laguna, P., Phinney, E. S., & Mészáros, P., 2004, *ApJ*, 615, 855
Kochanek, C. S., Dai, X., Morgan, C., Morgan, N., & Poindexter, S. C. G., 2007, Astronomical Society of the Pacific Conference Series, 371, 43
Kocsis, B., Frei, Z., Haiman, Z., & Menou, K., 2006, *ApJ*, 637, 27
Kollmeier, J. A. et al., 2006, *ApJ*, 648, 128
Komossa, S., Burwitz, V., Hasinger, G., Predehl, P., Kaastra, J. S., & Ikebe, Y., 2003, *ApJL*, 582, L15
Komossa, S., Halpern, J., Schartel, N., Hasinger, G., Santos-Lleo, M., & Predehl, P., 2004, *ApJL*, 603, L17
Koo, D. C., Kron, R. G., & Cudworth, K. M., 1986, *PASP*, 98, 285
Lacy, M., & SERVS team, 2009, Bulletin of the American Astronomical Society, Vol. 214, The Spitzer Extragalactic Representative Volume Survey (SERVS) - fields and coverages. p. 408.01
Leighly, K. M., Halpern, J. P., Jenkins, E. B., & Casebeer, D., 2007, *ApJS*, 173, 1
Lewis, G. F., Irwin, M. J., Hewett, P. C., & Foltz, C. B., 1998, *MNRAS*, 295, 573
Lidz, A., Hopkins, P. F., Cox, T. J., Hernquist, L., & Robertson, B., 2006, *ApJ*, 641, 41
Lonsdale, C. J. et al., 2003, *PASP*, 115, 897
Lundgren, B. F., Wilhite, B. C., Brunner, R. J., Hall, P. B., Schneider, D. P., York, D. G., Vanden Berk, D. E., & Brinkmann, J., 2007, *ApJ*, 656, 73
Luo, B., Brandt, W. N., Steffen, A. T., & Bauer, F. E., 2008, *ApJ*, 674, 122
Maddox, N., Hewett, P. C., Warren, S. J., & Croom, S. M., 2008, *MNRAS*, 386, 1605
Mainieri, V., Bergeron, J., Hasinger, G., Lehmann, I., Rosati, P., Schmidt, M., Szokoly, G., & Della Ceca, R., 2002, *A&A*, 393, 425
Martin, D. C. et al., 2005, *ApJL*, 619, L1
Martini, P., & Schneider, D. P., 2003, *ApJL*, 597, L109

Michelson, P. F., 2003, Society of Photo-Optical Instrumentation Engineers (SPIE) Conference Series, Vol. 4851, Instrumentation for the Gamma-ray Large Area Space Telescope (GLAST) mission, J. E. Truemper & H. D. Tananbaum, eds. pp. 1144–1150
Milosavljević, M., Merritt, D., & Ho, L. C., 2006, *ApJ*, 652, 120
Milosavljević, M., & Phinney, E. S., 2005, *ApJL*, 622, L93
Mineshige, S., & Yonehara, A., 1999, *PASJ*, 51, 497
Morgan, C. W., Eyler, M. E., Kochanek, C. S., Morgan, N. D., Falco, E. E., Vuissoz, C., Courbin, F., & Meylan, G., 2008, *ApJ*, 676, 80
Myers, A. D. et al., 2006, *ApJ*, 638, 622
Netzer, H., & Peterson, B. M., 1997, *Astrophysics and Space Science Library*, 218, 85
O'Neill, P. M., Nandra, K., Papadakis, I. E., & Turner, T. J., 2005, *MNRAS*, 358, 1405
Ouchi, M. et al., 2005, *ApJL*, 635, L117
Padmanabhan, N., White, M., Norberg, P., & Porciani, C., 2008, ArXiv e-prints, 0802.2105
Pereyra, N. A., Vanden Berk, D. E., Turnshek, D. A., Hillier, D. J., Wilhite, B. C., Kron, R. G., Schneider, D. P., & Brinkmann, J., 2006, *ApJ*, 642, 87
Perlman, E. S., Padovani, P., Landt, H., Stocke, J. T., Costamante, L., Rector, T., Giommi, P., & Schachter, J. F., 2001, in Astronomical Society of the Pacific Conference Series, Vol. 227, Blazar Demographics and Physics, P. Padovani & C. M. Urry, eds., p. 200
Peterson, B. M., 1993, *PASP*, 105, 247
Poindexter, S., Morgan, N., & Kochanek, C. S., 2008, *ApJ*, 673, 34
Polletta, M. d. C. et al., 2006, *ApJ*, 642, 673
Pooley, D., Blackburne, J. A., Rappaport, S., & Schechter, P. L., 2007, *ApJ*, 661, 19
Pooley, D., Blackburne, J. A., Rappaport, S., Schechter, P. L., & Fong, W.-f., 2006, *ApJ*, 648, 67
Popović, L. Č., & Chartas, G., 2005, *MNRAS*, 357, 135
Popović, L. Č., Mediavilla, E. G., Jovanović, P., & Muñoz, J. A., 2003, *A&A*, 398, 975
Qian, B., & Tao, J., 2004, *PASP*, 116, 161
Richards, G. T. et al., 2005, *MNRAS*, 360, 839
—, 2001, *AJ*, 121, 2308
—, 2003, *AJ*, 126, 1131
—, 2006a, *ApJS*, 166, 470
—, 2009, *ApJS*, 180, 67
—, 2006b, *AJ*, 131, 2766
Risaliti, G., Elvis, M., Fabbiano, G., Baldi, A., Zezas, A., & Salvati, M., 2007, *ApJL*, 659, L111
Rodriguez, C., Taylor, G. B., Zavala, R. T., Peck, A. B., Pollack, L. K., & Romani, R. W., 2006, *ApJ*, 646, 49
Roos, N., 1992, *ApJ*, 385, 108
Ross, N. P. et al., 2009, ArXiv e-prints, 0903.3230
Rosswog, S., Ramirez-Ruiz, E., & Hix, W. R., 2008, *ApJ*, 679, 1385
Sandage, A., 1965, *ApJ*, 141, 1560
Sanders, D. B. et al., 2007, *ApJS*, 172, 86
Saxton, R. D., Read, A. M., Esquej, P., Freyberg, M. J., Altieri, B., & Bermejo, D., 2008, *A&A*, 480, 611
Schmidt, M., 1963, *Nature*, 197, 1040
—, 1968, *ApJ*, 151, 393
Schmidt, M., & Green, R. F., 1983, *ApJ*, 269, 352
Schmidt, M. et al., 1998, *A&A*, 329, 495
Schneider, D. P. et al., 2007, *AJ*, 134, 102
Schneider, P., Ehlers, J., & Falco, E. E., 1992, Gravitational Lenses, P. Schneider, J. Ehlers, & E. E. Falco, eds.
Scoville, N. et al., 2007, *ApJS*, 172, 1
Sesana, A., Vecchio, A., Eracleous, M., & Sigurdsson, S., 2008, *MNRAS*, 391, 718
Sesar, B. et al., 2007, *AJ*, 134, 2236
—, 2006, *AJ*, 131, 2801
Shen, Y., Greene, J. E., Strauss, M. A., Richards, G. T., & Schneider, D. P., 2008a, *ApJ*, 680, 169
Shen, Y. et al., 2007, *AJ*, 133, 2222
—, 2008b, ArXiv e-prints, 0810.4144
Skrutskie, M. F. et al., 2006, *AJ*, 131, 1163
Stalin, C. S., Gupta, A. C., Gopal-Krishna, Wiita, P. J., & Sagar, R., 2005, *MNRAS*, 356, 607
Steffen, A. T., Strateva, I., Brandt, W. N., Alexander, D. M., Koekemoer, A. M., Lehmer, B. D., Schneider, D. P.,

& Vignali, C., 2006, *AJ*, 131, 2826
Sutherland, W., 2009, in Science with the VLT in the ELT Era, A. Moorwood, ed., p. 171
Tao, J., Fan, J., Qian, B., & Liu, Y., 2008, *AJ*, 135, 737
Tremaine, S. et al., 2002, *ApJ*, 574, 740
Trèvese, D., Kron, R. G., & Bunone, A., 2001, *ApJ*, 551, 103
Truemper, J., 1982, *Advances in Space Research*, 2, 241
Ueda, Y., Akiyama, M., Ohta, K., & Miyaji, T., 2003, *ApJ*, 598, 886
Ulmer, A., 1999, *ApJ*, 514, 180
Uttley, P., & Mchardy, I. M., 2004, *Progress of Theoretical Physics Supplement*, 155, 170
Valtonen, M. J., 2007, *ApJ*, 659, 1074
Valtonen, M. J. et al., 2008, *Nature*, 452, 851
Vanden Berk, D. E. et al., 2004, *ApJ*, 601, 692
Vaughan, S., Edelson, R., & Warwick, R. S., 2004, *MNRAS*, 349, L1
Voges, W. et al., 1999, *A&A*, 349, 389
Volonteri, M., 2008, Evolution of Supermassive Black Holes, B. Aschenbach, V. Burwitz, G. Hasinger, & B. Leibundgut, eds. p. 174
Wang, J., & Merritt, D., 2004, *ApJ*, 600, 149
Weinstein, M. A. et al., 2004, *ApJS*, 155, 243
White, M., Martini, P., & Cohn, J. D., 2008, *MNRAS*, 390, 1179
Wilhite, B. C., Vanden Berk, D. E., Brunner, R. J., & Brinkmann, J. V., 2006, *ApJ*, 641, 78
Wilhite, B. C., Vanden Berk, D. E., Kron, R. G., Schneider, D. P., Pereyra, N., Brunner, R. J., Richards, G. T., & Brinkmann, J. V., 2005, *ApJ*, 633, 638
Wolf, C., Wisotzki, L., Borch, A., Dye, S., Kleinheinrich, M., & Meisenheimer, K., 2003, *A&A*, 408, 499
Wyithe, J. S. B., & Loeb, A., 2002, *ApJ*, 581, 886
Yonehara, A., Mineshige, S., Fukue, J., Umemura, M., & Turner, E. L., 1999, *A&A*, 343, 41
York, D. G. et al., 2000, *AJ*, 120, 1579
Yu, Q., 2002, *MNRAS*, 331, 935
Zakamska, N. L. et al., 2003, *AJ*, 126, 2125
Zehavi, I. et al., 2005, *ApJ*, 630, 1